BRAIN PRODUCTS
Solutions for neurophysiological research

EEG & fMRI

BRAIN PRODUCTS
Solutions for neurophysiological research

Contents

Abstract

Much of the motivation to explore simultaneously recorded EEG-fMRI comes from the complementary nature of the neurophysiological activity provided by each of the recording modalities. fMRI has precise spatial resolution, but suffers from poor temporal resolution; whereas, the opposite is true for EEG, insofar as EEG has high temporal resolution with less precise spatial resolution than fMRI.

Due to the complementary strengths and weaknesses of each of these recording modalities, combining EEG-fMRI has fostered a deeper understanding of the structure and function of the brain. Over the years simultaneous EEG-fMRI has been used in a broad range of applications including sleep, epilepsy, cognition, brain stimulation, neurofeedback, and brain connectome studies. Through advancements in technology, data analytics, and artifact handling, simultaneous EEG-fMRI has emerged as a robust application that continues to contribute to the understanding of the brain.

Since the inception of the first MR-compatible EEG amplifier in 2000, Brain Products remains at the forefront of EEG-fMRI research by offering the best solutions for recording EEG-fMRI data with the highest data quality and safety standards. This booklet is designed to introduce you to the solutions offered by Brain Products and highlight possible applications including combining non-neural physiological recordings with EEG-fMRI.

The broad spectrum of simultaneous EEG-fMRI applications:

More and more researchers are realizing the power of a combined EEG-fMRI approach. EEG and fMRI complement each other on a spatial and temporal scale and offer different perspectives on brain function. However, simultaneous EEG-fMRI presents some challenges in acquiring and analyzing the data that may not be necessary for every study. An article by Scrivener 2021 provides helpful study guidelines when considering combined EEG-fMRI [1].

Simultaneous EEG-fMRI studies are particularly informative in situations where data acquired from one modality can be used to make inferences about the signal properties of the other modality because the data is acquired exactly at the same moment. Here we will give an overview of some common applications, a review of further applications can be found in Warbrick 2022 [2].

Epilepsy: An excellent example of when EEG and fMRI data must be acquired at the same moment is the study of epilepsy. Epileptic patients generate interictal spikes between seizures. These spikes are believed to be generated by the same sources as the seizures themselves. Therefore, the ability to localize the source of the spike will help considerably in gaining a better understanding of epilepsy. In order to localize the interictal spike, it is necessary to know at what moment it occurs. A patient cannot generate these spikes at will, so they must be located retrospectively. It is therefore essential to record EEG activity in parallel with fMRI scanning.

The interictal spikes have a large amplitude and therefore yield a high ratio of signal to noise. However, the shape of the spikes varies, and movement artifacts in the scanner can confound the data. With the integration of our Carbon Wire Loops, artifacts arising from head movement and cardiac cycle-related arterial pulsing in the scanner can easily be removed from the data and help increase the signal to noise ratio for small temporal spikes [3]. Simultaneous EEG-fMRI serves as a non-invasive application for localizing interictal epileptic discharges and studying their propagation [4].

Perception: Sensory perception is an example of a behavioral paradigm in which the stimulus predicts the response; however, the behavioral response to an external stimulus does not occur in isolation and behavior varies across individuals. Neural oscillations have been implicated in coordinating neural communication during perception and can explain the variability in both behavior and the hemodynamic response across individuals. Simultaneous EEG-fMRI allows for the spatial localization of changes in distinct neural frequency bands involved in perception. For example, a study involving simultaneous EEG and high-resolution fMRI showed during attended trials, alpha and beta power correlated negatively with the BOLD signal in deep layers, while gamma activity correlated positively with the BOLD signal in superficial layers [5].

In addition, Warbrick et al found that the P1 component of the ERP reflects changes in the sensory encoding of a stimulus, and this can be used to model sensory encoding related BOLD responses, illustrating how perceptual

measures in the EEG can be integrated in the fMRI data analysis [6].

Resting state: What is the brain doing when it is not performing a task? This is a crucial question, because much of the brain's metabolism is responsible for maintaining the brain in a state of readiness rather than being expended on task execution. fMRI studies have demonstrated the presence of functional networks in the brain that are active during resting state. The connection between EEG rhythms and the resting-state networks can be established with simultaneous EEG-fMRI. For example, it has been demonstrated that ongoing brain activity consists of metastable microstates that can be distinguished by their EEG signatures and are associated with certain default brain networks [7]. Furthermore, time-varying functional connectivity in simultaneous EEG-fMRI studies has revealed the neuronal activity underlying the fMRI resting-state networks are linked with EEG frequency bands and allows for studying functional reorganization of networks on different time scales [8]. Concurrent TMS-EEG-fMRI has also been implemented to causally study the network dynamics of distinct frequency bands [9]. Additionally, transcranial modulation of the alpha band using tACS has been shown to result in stronger connectivity in the default mode network [10].

Sleep: An important special case of the resting state is sleep. Picchioni and colleagues correlated the oscillations in the infraslow range (< 0.1 Hz) with fMRI and discovered that during sleep the correlation is positive in subcortical areas, but negative in cortical areas [11]. Sämann and colleagues used EEG in the scanner to monitor the different sleep stages and to follow the changes in the default-mode network through successive stages [12]. Brain Products' BrainVision RecView software was used for online monitoring of the sleep stages [5]. Recently, simultaneous EEG-fMRI has demonstrated that differences in brain activation time-locked to sleep spindles correlated with variability in cognitive abilities. [13], further illustrating that simultaneous EEG- fMRI is a powerful tool in sleep research.

Cognitive control: Task execution depends on cognitive control. During an experimental task subjects will monitor their performance and adjust it according to feedback. A variety of ERP components, such as N2, P3, ERN and CNV are known to be cognitive control task performance markers. Using the single-trial amplitude of those components as regressors in fMRI analysis helps to dissociate the respective roles of different brain networks during cognitive control tasks [14] [15]. For example, Karch and colleagues looked at the brain areas that correlated to the single-trial amplitudes of the N2 and P3 components of ERPs during the voluntary selection stage in a modified Go-NoGo task [16] . Scheibe and colleagues used the modulation of single-trial CNV variation to reveal the brain areas that were sensitive to prior probability in the stimuli during decision-making [17]. Simultaneous EEG-fMRI can also be used to provide real-time measures of brain activity for neurofeedback. Patients with major depressive disorder used neurofeedback training to upregulate frontal alpha and beta band activity associated with reduced anhedonia and anxiety [18].

We have only highlighted a few applications in which simultaneous EEG-fMRI added valuable insight. Other applications of EEG-fMRI in recent years have involved memory, pain, somatosensory perception and ADHD, but the spectrum of possible applications is not restricted to this list. Your ideas can contribute to the field. For our part, we can assure you that the equipment you might need is already available for you to use.

Non-EEG sensors add new dimensions to brain research

The combination of EEG and fMRI opens a window into brain function; however, non-neural physiological signals provide further insight into the connection between the brain and body.

Aberrant motor control and tremors are physiological symptoms of many neurological illnesses that can be assessed with electromyography (EMG). Dirkx and colleagues showed that the tremor amplitude in Parkinson's patients correlated with network activity associated with the basal ganglia in a combined EMG-fMRI study [19]. Altered sensorimotor gaiting of the startle response, measured with EMG in patients with Tourette Syndrome resulted in decreased BOLD activity [20].

Shitara and colleagues recorded EMG during TMS stimulation inside the scanner. The EMG made it possible to discriminate the sub- and suprathreshold TMS activations. Accordingly, the authors could demonstrate differences in the fMRI responses between sub- and supra threshold fMRI activations [21] [9].

Galvanic skin response (GSR) measurement is an essential tool in studies of classical conditioning. Spoormaker and colleagues measured GSR inside the scanner in a fear-conditioning paradigm [22]. The increase in GSR was used as a marker of successful conditioning. In a further application of the same paradigm, the authors introduced a period of sleep between fear conditioning sessions.

GSR in conjunction with the fMRI results confirmed the hypothesis that REM sleep has a positive role in fear extinction[23].

Respiration is a critical factor to consider in the MR environment. Respiration rate impacts both the hemodynamic properties of the BOLD signal as well as induced movement related artifacts. Studies have shown different respiration rates are linked to changes in BOLD activity and may confound resting state studies [24]. Simultaneous recording of respiration rate with EEG-fMRI using our Respiration Belt MR, for example, can be used for efficient respiration-related artifact correction in both data modalities. Moreover, a parallel-acquired respiration signal can also be used to explain variations in the BOLD signal. One example where changes in the BOLD signal are tightly linked to autonomic physiology is during sleep. Changes in respiration rate and heart rate are correlated with alteration in resting-state functional connectivity during the onset of sleep [25].

Besides these example, other novel applications are being tried, such as the use of accelerometry for measuring limb movements. The increase in the inclusion of non-EEG sensors in EEG-fMRI studies is an encouraging trend. We at Brain Products strongly believe that using auxiliary sensors to monitor peripheral physiological responses will add weight to the results of many fMRI or EEG-fMRI studies.

References

[1] C. L. Scrivener, „When Is Simultaneous Recording Necessary? A Guide for Researchers Considering Combined EEG-fMRI," vol. 15, p. 636424, 2021.

[2] T. Warbrick, „Simultaneous EEG-fMRI: What Have We Learned and What Does the Future Hold?," Sensors, vol. 22, no. 6, p. 2262, 2022.

[3] N. Von Ellenrieder, N. Zazubovits and J. Gotman, „Carbon Wire Loops in EEG-fMRI studies of interictal epileptic activity," Brain Products, 4 December 2020. [Online]. Available: https://pressrelease.brainproducts.com/cwl-ux-montreal/. [Accessed 17 March 2022].

[4] H. M. Khoo, N. von Ellenrieder, N. Zazubovits, D. He, D. Francois and J. Gotman, „The spike onset zone. The region where epileptic spikes start and from where they propogate," Neurology, vol. 91, no. 7, p. e666−e674, 2018.

[5] R. Scheeringa, P. J. Koopmas, T. Van Morik, O. Jensen and D. G. Norris, „The relationship between oscillatory EEG activity and the laminar-specific BOLD signal," PNAS, vol. 113, no. 24, 2016.

[6] T. Warbrick, J. Arrubla, F. Boers, I. Neuner and N. Shah, „Attention to detail: why considering task demands is essential for single-trial analysis of BOLD correlates of the visual P1 and N1," Cogn Neurosci, pp. 529-42, 2014.

[7] F. Musso, J. Brinkmeyer, A. Mobascher, T. Warbrick and G. Winterer, „Spontaneous brain activity and EEG microstates. A novel EEG-fMRI analysis approach to explore resting-state networks," NeuroImage, vol. 52, no. 4, pp. 1149-1161, 2010.

[8] J. Wirsich, A.-L. Giraud and S. Sadaghiani, „Concurrent EEG- and fMRI-derived functional connectomes exhibit linked dynamics," NeuroImage, vol. 219, p. 116998, 2020.

[9] J. C. Peters, J. Reithler, T. A. de Graaf, T. Schumann, R. Goebel and A. T. Sack, „Concurrent human TMS-EEG-fMRI enables monitoring of oscillatory brain state-dependent gating of cortico-subcortical network activity," Communications Biology, vol. 3, no. 40, 2020.

[10] K. J. Clancy, J. A. Andrzejewski, Y. You, J. T. Rosenberg, M. Ding and W. Li, „Transcranial stimulation of alpha oscillations up-regulates the default mode network," PNAS, vol. 119, no. 1, p. e2110868119, 2021.

[11] D. W. Picchioni Carr, J. Meltzer, T. Balkin, J. Duyn and A. Braun, „Infraslow EEG oscillations organize large-scale cortical-subcortical interactions during sleep: a combined EEG-fMRI study," Brain Res , vol. 1374, pp. 63-72., 2011.

[12] P. Sämann, R. Wehrle, D. Hoehn, V. Spoormaker, H. Peters, C. Tully, F. Holsboer and M. Czisch, „Development of the Brain's Default Mode Network from Wakefulness to Slow Wave Sleep.," Cereb Cortex , vol. 21, no. 9, pp. 2082-93, 2011.

[13] Z. Fang, L. B. Ray, A. M. Owen and S. M. Fogel, „Brain Activation Time-Locked to Sleep Spindles Associated with Human Cognitive Abilities," Frontiers in Neuroscience, vol. 13, no. 46, 2019.

[14] S. Debener, M. Ullsperger, M. Siegel and A. K. Engel, „Single-trial EEG-fMRI reveals the dynamics of cognitive function," Trends Cogn Sci, vol. 10, no. 12, pp. 558-63, 2006.

[15] T. Eichele, K. Specht, . M. Moosmann, . M. L. Jongsma, R. Q. Quiroga, H. Nordby and K. Hugdahl, „Assessing the spatiotemporal evolution of neuronal activation with single-trial event-related potentials and functional MRI," PNAS, vol. 102, no. 49, 2005.

[16] S. Karch, R. Feuerecker, G. Leicht, T. Meindl, I. Hantschk, V. Kirsch, M. Ertl, J. Lutz, O. Pogarell and C. Mulert, „Separating distinct aspects of the voluntary selection between response alternatives: N2- and P3-related BOLD responses.," NeuroImage, vol. 51, no. 1, pp. 356-364, 2010.

[17] C. Scheibe, M. Ullsperger, W. Sommer and H. Heekeren, „Effects of parametrical and trial-to-trial variation in prior probabiltiy processing revealed by simultaneous electroenecephalogra/functional magnetic resonace imaging," J Neurosci, vol. 30, no. 49, pp. 16709-17, 2011.

[18] V. Zotev and J. Bodurka, „Effects of simultaneous real-time fMRI and EEG neurofeedback in major depressive disorder evaluated with brain electromagnetic tomography," NeuroImage Clin, vol. 28, p. 102459, 2020.

[19] M. Dirkx, d. O. H. E. Aarts, M. Timmer, B. Bloem, I. Toni and R. Helmich, „The Cerebral Network of Parkinson's Tremor: An Effective Connectivity fMRI Study.," J Neurosci, vol. 36, no. 19, pp. 5362-72, 2016.

[20] J. Buse, C. Beste, E. Herrmann and V. Roessner, „Neural correlates of altered sensorimotor gating in boys with Tourette Syndrome: A combined EMG/fMRI study," Worl J Biol Psychiatry, vol. 17, no. 3, pp. 187-97, 2016.

[21] H. Shitara, T. Shinozaki, K. Takagishi, M. Honda and T. Hanakawa, „Time course and spatial distribution of fMRI signal changes during single-pulse transcranial magnetic stimulation to the primary motor cortex.," NeuroImage, vol. 56, no. 3, pp. 1469-79, 2011.

[22] V. Spoormaker, A. Sturm, K. Andrade, M. Schroter, R. Goya-Maldonado, F. Holsboer, T. Wetter and P. C. M. Samann, „The neural correlates and temporal sequence of the relationship between shock exposure, disturbed sleep and impaired consolidation," J Psychiatr Res, vol. 44, no. 16, pp. 1121-8, 2010.

[23] V. I. Spoormaker, K. C. Andrade, M. S. Schroter, A. Sturm, R. Goya-Maldonado, P. G. Samann and M. Czisch, „The neural correlates of negative prediction error signaling in human fear conditioning," NeuroImage, vol. 54, no. 3, pp. 2250-6, 2011.

[24] M. E. Thomason, B. E. Burrows, J. D. Gabrieli and G. H. Glover, „Breath holding reveals differences in fMRI BOLD signal in children and adults," NeuroImage, vol. 25, no. 3, pp. 824-37, 2005.

[25] C. S. Soon, K. Viongradova, J. L. Ong, V. D. Calhoun, T. Liu, J. H. Zhou, K. K. Ng and M. W. Chee, „Respiratory, cardiac, EEG, BOLD signals and functional connectivity over multiple microsleep episodes," NeuroImage, vol. 237, p. 118129, 2021.

User Research Articles

Our community of customers is highly productive when it comes to publishing quality research. We are always happy to hear about the papers our customers publish and we like to feature user research in our press releases. In recent years, many cutting edge simultaneous EEG-fMRI papers have been published by our customers. Here, we present some examples of the papers we have featured in our press releases. The user research covers diverse simultaneous EEG-fMRI applications and each one advances knowledge in their respective research field: EEG-fMRI in pre-term infants (Tom Arichi and Lorenzo Fabrizi, London UK), artifact handling and safety in ultra-high magnetic fields (Joao, Jorge, Lausanne, Switzerland), cortical and subcortical processing during sleep (Andrew Bagshaw, Birmingham UK), and a trimodal imaging approach using EEG, MR and PET (Jon Shah, Ravi Rajkumar and Irene Neuner, Juelich, Germany).

Simultaneous EEG-fMRI provides a new insight into the origin of spontaneous neuronal activity in preterm humans

by Tomoki Arichi[1,2] and Lorenzo Fabrizi[3]
[1]Centre for the Developing Brain, Division of Imaging Sciences and Biomedical Engineering, King's College London, St Thomas' Hospital, London, SE1 7EH, UK
[2]Department of Bioengineering, Imperial College London, South Kensington Campus, London, SW7 2AZ, UK
[3]Department of Neuroscience, Physiology & Pharmacology, University College London, Gower Street, London, WC1 E6BT, UK

Acknowledgement

Introduction

During the third trimester of human gestation (28 to 40 weeks post-menstrual age (PMA)), the brain undergoes a sequence of functional and structural maturational changes as the cortex and its underlying framework of connectivity are established. The importance of this period is emphasised by the greater risk of adverse neurodevelopmental outcome in infants delivered preterm (prior to 37 weeks PMA) [1, 2].

In animal models, spontaneous bursts of synchronized activity (known as spindle bursts) play an instructive role in the developmental processes that set early cortical circuits [3-5]. In keeping with this, experimental disruption of the normal occurrence and propagation of early spontaneous patterned activity leads to permanent loss of healthy cortical organization [6, 7]. Similarly, neural activity recorded in preterm human infants with electroencephalography (EEG) is characterized by intermittent high amplitude bursts which can occur both spontaneously and following external stimulation [4, 8, 9]. The most common of these events is the delta brush, a transient pattern characterised by a slow delta wave (1-4Hz) with a superimposed fast frequency spindle (8-25Hz) [8]. This pattern appears to represent a key marker of healthy neuronal development as their persistence at term equivalent age (or an earlier absence) correlates with underlying brain injury and/or adverse neurological outcome later in childhood [10]. However, despite the common occurrence, developmental importance and clinical significance of delta brushes, the brain structures which generate this hallmark neuronal pattern within the developing human brain remain unknown.

While the time of occurrence and the scalp distribution of a delta brush event can

be readily identified with EEG, the spatial localization of its source cannot be inferred with certainty just from the electrical potentials recorded at the scalp surface. To overcome this intrinsic limitation of EEG recording, we pioneered the use of simultaneous EEG-fMRI in human neonates. Recent research has explored the direct correlation between neural and hemodynamic function in adult humans with this method, demonstrating the potential insights it can provide in both health and pathology. For example, EEG-fMRI has been employed to identify the source of epileptogenic EEG activity in presurgical planning [11], to investigate the association between spontaneous EEG oscillations and fMRI fluctuations at rest [12] or in cognitive neuroscience to localise the source of task-related event related potentials [13, 14]. However, the coupling between resting neuronal and hemodynamic activity has never been explored in the developing infant brain. Here, we provide the first evidence that spontaneous patterns of delta brush activity in the preterm period are associated with significant hemodynamic activity clearly localized to distinct regions within the developing cortex.

Methods

Participants

Thirteen preterm infants (five females; studied between 32-36 weeks post-menstrual age, PMA) 5-55 days old (23 ± 17, mean ± SD) from the Neonatal Unit at St Thomas' Hospital, London, participated in this study. Informed written parental consent was obtained prior to each study.

All of the research methods conformed to the standards set by the Declaration of Helsinki and was approved by the National Research Ethics Committee.

EEG-fMRI aquisition

MR images were collected during sleep on a 3-Tesla Philips Achieva scanner (Best, Netherlands). Concurrent EEG recording were conducted with a custom-made BrainCap MR sized for the head of preterm infant containing 26-32 scalp electrodes (EASYCAP GmbH, DE) connected to an MR-compatible EEG system (BrainAmp MR, Brain Products GmbH, DE).

EEG-fMRI pre-processing and analysis

Gradient artefacts caused by the MR image acquisition in the EEG were corrected using Analyzer 2 software (Brain Products, DE). The typical EEG cardioballistic artefacts were not present in our neonatal recordings. fMRI standard pre-processing was performed using FSL (FMRIB's software library, www.fmrib.ox.ac.uk/fsl) [15]. Residual motion and physiological noise were removed with Probabilistic Independent Component Analysis [PICA, v3.0] [16].

Three independent trained observers reviewed the EEG recordings and marked the occurrence of delta brush events on the same software. Events were then labelled based on their field distribution and used as separate Explanatory Variables (EVs) in the general linear model (GLM) of the fMRI analysis to generate spatial maps of activated voxels at an individual subject level. Only EVs

containing more than 3 events during the acquisition period were used for analysis. Individual subject activation maps were then co-aligned to an age-specific neonatal atlas for group analysis.

Results

Simultaneous EEG-fMRI was successfully acquired in 10 of the 13 infants over a median of 7.5 minutes (range: 3.5-10.5 minutes).

A median of 4.4 delta brushes per minute (range: 1.9 – 6.7) with a total of 23 distinct topographical distributions were found across all subjects. However, only 10 topographies occurred more than three times in a given subject and were included in the fMRI analysis (Figure 1). These covered the parietal, occipital and temporal, but not frontal areas of the scalp.

We then found that different delta brush topographies were associated with different BOLD activity maps at subject level. When significant areas of BOLD activity were present, this always included at least one cluster ipsilateral to the side of the recorded delta brush activity. As most of the delta brushes in our study consistently occurred over the left (n = 78 from 9/10 subjects) and right (n = 86 from 10/10 subjects) posterior. temporal regions, the corresponding single subject data were taken forward to group analysis. Lateralized posterior-temporal
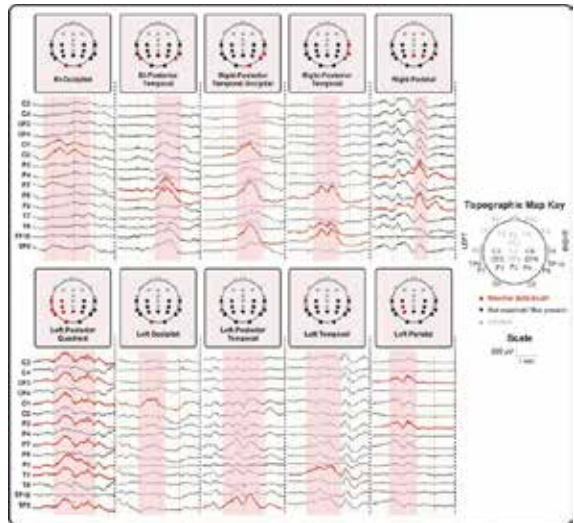

Figure 1. Examples of delta brushes with different topographies recorded in the MR scanner and after gradient artefact removal.

delta brush activity was associated on both a single subject and group level with significant clusters of positive BOLD activity in the insular cortex ipsilateral to the delta brush activity (Figure 2). Right-sided delta brush activity was also associated with significant clusters of hemodynamic activity in the right superior temporal cortex and extending to the right temporal pole (Figure 2).

Discussion

The human preterm EEG is characterised by spontaneous neuronal bursts, which in animals are known to be crucial for cortical development. Here we have shown that these are organized into a set of spatiotemporal patterns, the most common of which has a unilateral posterior-temporal scalp distribution in the period equivalent to
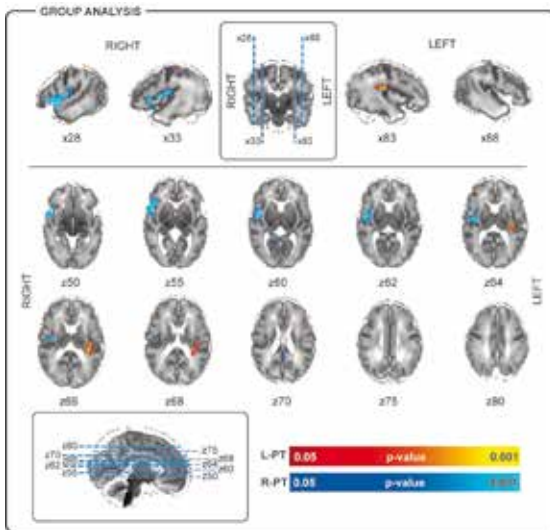
Figure 2. BOLD activity associated with the occurrence of left posterior-temporal (L-PT) and right posterior-temporal (R-PT) delta brushes.

the last trimester of gestation. These bursts are associated with ipsilateral clusters of hemodynamic activation in the insular cortex only and insular and temporal cortices when occurring over the left and right hemispheres respectively.

As hypothesised, the simultaneous acquisition of EEG-fMRI data proved to be highly complementary, permitting the source localization of the delta brush activity, not previously achieved. By taking advantage of natural sleep, we were able to successfully record data for analysis in 10 of the 13 subjects studied. This approach allowed us to identify specific developmental patterns of spontaneous neural activity with EEG and subsequently link this activity directly to the whole-brain spatial information offered by

fMRI, combining the strengths of these two techniques and overcoming their individual limitations.

The incidence and topographical distribution of the delta brush changes across the preterm period. Over this period, delta brushes can also be elicited by external sensory stimuli [10] and their topography is related to the stimulus modality: visual, auditory and tactile stimulation evoke occipital, mid-temporal and pericentral delta brushes [17-19]. These observations suggest that delta brushes with different topographies (whether spontaneous or evoked) are related to distinct brain functions which develop in different time frames. Our discovery here, that spontaneous posterior-temporal delta brushes arise in the insula and temporal pole, has therefore important implications for understanding the events underlying brain development in the preterm infant.

The mature insula is a structural and functional hub with a dense pattern of connectivity to almost all other regions of the brain, enabling it to play a versatile role in a wide range of functions including sensory and pain perception, emotion, and cognition [20]. As in humans, the insula plays an important multisensory role also in adult rodents [21].

This function develops in the third postnatal week (equivalent to the late preterm period in humans) with the maturation of inhibitory circuits and an optimal excitation/inhibition balance [22], however nothing is known about its spontaneous activity as most of these kind of recordings have been from the primary sensory cortices. Our results suggest that it could be important to record from this area as it may represent a major source of early neuronal bursting activity in rodents as well as in humans.

Our findings are of further significance in light of the increasing number of studies using fMRI to characterize developmental changes in resting state functional connectivity and task-induced responses in early infancy [23]. Despite marked maturational changes in early life in the neurovascular coupling cascade [24, 25], we demonstrate for the first time in this population, a clear association between a direct measure of neural activity (EEG) and functional hemodynamic activity as measured by fMRI.

This provides the potential to understand hemodynamic fluctuations in terms of the underlying neuronal rhythms and, in particular, to link connectivity measures across the two modalities [26]. Although the majority of resting state networks at term equivalent age are spatially similar to those observed in adults [27, 28] their role and underlying neuronal processes may differ.

This study provides the first evidence that spontaneous bursting neuronal activity, and specifically the delta brush, is largely generated by the insula in the late human preterm period. The insula is a phylogenetically ancient part of the brain that undergoes dramatic functional and structural maturation at this time, preceding that of the overlying neocortex. Since the equivalent of the delta brush in rodents has an instructive function in the normal neuronal maturation of the cortex, we propose that the insula plays a key developmental role as generator of such activity in early human life.

References

[1] Allen, M.C. (2008). Neurodevelopmental outcomes of preterm infants. Curr Opin Neurol. 21, 123-128.

[2] Larroque, B., Ancel, P.Y., Marret, S., Marchand, L., Andre, M., Arnaud, C., Pierrat, V., Roze, J.C., Messer, J., Thiriez, G., et al. (2008). Neurodevelopmental disabilities and special care of 5-year-old children born before 33 weeks of gestation (the EPIPAGE study): a longitudinal cohort study. Lancet 371, 813-820.

[3] Hanganu-Opatz, I.L. (2010). Between molecules and experience: role of early patterns of coordinated activity for the development of cortical maps and sensory abilities. Brain Res Rev 64, 160-176.

[4] Khazipov, R., and Luhmann, H.J. (2006). Early patterns of electrical activity in the developing cerebral cortex of humans and rodents. Trends Neurosci 29, 414-418.

[5] Rakic, P., and Komuro, H. (1995). The role of receptor/channel activity in neuronal cell migration. J Neurobiol 26, 299-315.

[6] Xu, H.P., Furman, M., Mineur, Y.S., Chen, H., King, S.L., Zenisek, D., Zhou, Z.J., Butts, D.A., Tian, N., Picciotto, M.R., et al. (2011). An Instructive role for patterned spontaneous retinal activity in mouse visual map development. Neuron 70, 1115-1127.

[7] Tolner, E.A., Sheikh, A., Yukin, A.Y., Kaila, K., and Kanold, P.O. (2012). Subplate neurons promote spindle bursts and thalamocortical patterning in the neonatal rat somatosensory cortex. J Neurosci 32, 692-702.

[8] Andre, M., Lamblin, M.D., d'Allest, A.M., Curzi-Dascalova, L., Moussalli-Salefranque, F., T, S.N.T., Vecchierini-Blineau, M.F., Wallois, F., Walls-Esquivel, E., and Plouin, P. (2010). Electroencephalography in premature and full-term infants. Developmental features and glossary. Neurophysiol Clin 40, 59-124.

[9] Tolonen, M., Palva, J.M., Andersson, S., and Vanhatalo, S. (2007). Development of the spontaneous activity transients and ongoing cortical activity in human preterm babies. Neuroscience 145, 997-1006.

[10] Whitehead, K., Pressler, R., and Fabrizi, L. (2017). Characteristics and clinical significance of delta brushes in the EEG of premature infants. Clin Neurophys Prac 2, 12-18.

[11] Gotman, J., and Pittau, F. (2011). Combining EEG and fMRI in the study of epileptic discharges. Epilepsia 52 Suppl 4, 38-42.

[12] Laufs, H. (2008). Endogenous brain oscillations and related networks detected by surface EEG-combined fMRI. Hum Brain Map 29, 762-769.

[13] Huster, R.J., Debener, S., Eichele, T., and Herrmann, C.S. (2012). Methods for simultaneous EEG-fMRI: an introductory review. J Neurosci 32, 6053-6060.

[14] Ritter, P., and Villringer, A. (2006). Simultaneous EEG-fMRI. Neurosci. Biobehav Rev 30, 823-838.

[15] Smith, S.M., Jenkinson, M., Woolrich, M.W., Beckmann, C.F., Behrens, T.E., Johansen-Berg, H., Bannister, P.R., De Luca, M., Drobnjak, I., Flitney, D.E., et al. (2004). Advances in functional and structural MR image analysis and implementation as FSL. Neuroimage 23 Suppl 1, S208-219.

[16] Beckmann, C.F., and Smith, S.M. (2004). Probabilistic independent component analysis for functional magnetic resonance imaging. IEEE Trans Med Imaging 23, 137-152.

[17] Chipaux, M., Colonnese, M.T., Mauguen, A., Fellous, L., Mokhtari, M., Lezcano, O., Milh, M., Dulac, O., Chiron, C., Khazipov, R., et al. (2013). Auditory Stimuli Mimicking Ambient Sounds Drive Temporal "Delta-Brushes" in Premature Infants PloS one 8.

[18] Colonnese, M.T., Kaminska, A., Minlebaev, M., Milh, M., Bloem, B., Lescure, S., Moriette, G., Chiron, C., Ben-Ari, Y., and Khazipov, R. (2010). A conserved switch in sensory processing prepares developing neocortex for vision. Neuron 67, 480-498.

[19] Milh, M., Kaminska, A., Huon, C., Lapillonne, A., Ben-Ari, Y., and Khazipov, R. (2007). Rapid cortical oscillations and early motor activity in premature human neonate. Cereb. Cortex 17, 1582-1594.

[20] Nieuwenhuys, R. (2012). The insular cortex: a review. Prog. Brain Res 195, 123-163.

[21] Rodgers, K.M., Benison, A.M., Klein, A., and Barth, D.S. (2008). Auditory, somatosensory, and multisensory insular cortex in the rat. Cereb. Cortex 18, 2941-2951.

[22] Gogolla, N., Takesian, A.E., Feng, G., Fagiolini, M., and Hensch, T.K. (2014). Sensory integration in mouse insular cortex reflects GABA circuit maturation. Neuron 83, 894-905.

[23] Graham, A.M., Pfeifer, J.H., Fisher, P.A., Lin, W., Gao, W., and Fair, D.A. (2015). The potential of infant fMRI research and the study of early life stress as a promising exemplar. Developmental cognitive neuroscience 12, 12-39.

[24] Arichi, T., Fagiolo, G., Varela, M., Melendez-Calderon, A., Allievi, A., Merchant, N., Tusor, N., Counsell, S.J., Burdet, E., Beckmann, C.F., et al. (2012). Development of BOLD signal hemodynamic responses in the human brain. Neuroimage 63, 663-673.

[25] Harris, J.J., Reynell, C., and Attwell, D. (2011). The physiology of developmental changes in BOLD functional imaging signals. Dev Cog Neurosci 1, 199-216.

[26] Vanhatalo, S., and Fransson, P. (2016). Advanced EEG and MRI Measurements to Study the Functional Development of the Newborn Brain. In Prenatal and Postnatal Determinants of Development, D.W. Walker, ed. (New York: Springer New York), pp. 53-68.

[27] Doria, V., Beckmann, C.F., Arichi, T., Merchant, N., Groppo, M., Turkheimer, F.E., Counsell, S.J., Murgasova, M., Aljabar, P., Nunes, R.G., et al. (2010). Emergence of resting state networks in the preterm human brain. Proc Natl Acad Sci U S A 107, 20015-20020.

[28] Smyser, C.D., Inder, T.E., Shimony, J.S., Hill, J.E., Degnan, A.J., Snyder, A.Z., and Neil, J.J. (2010). Longitudinal analysis of neural network development in preterm infants. Cereb. Cortex 20, 2852-2862.

Simultaneous EEG-fMRI at ultra-high field: Artifact prevention and safety assessment

by João Jorge[1],[2]
[1]Laboratory for Functional and Metabolic Imaging, EPFL, Lausanne, Switzerland
[2]Institute for Systems and Robotics, IST, Lisbon, Portugal

Introduction

Simultaneous EEG-fMRI acquisitions can offer valuable insights for the non-invasive study of human brain function (Britz et al., 2010; Gotman and Pittau, 2011; Scheeringa et al., 2011). Concurrently, the benefits offered by high-field imaging, yielding super-linear gains in BOLD sensitivity (van der Zwaag et al., 2009), have attracted considerable interest towards simultaneous EEG-fMRI at higher field strengths (Neuner et al., 2013). Unfortunately, simultaneous acquisitions are subject to problematic interactions that can compromise data quality and subject safety. Safety concerns arise due to the possible generation of electric currents along the EEG wires, induced by the MRI gradients or RF pulses (Dempsey and Condon, 2001). This is increasingly problematic at higher field strengths such as 7T, where the RF pulse energy is higher and the wavelength becomes smaller than the sample size (Eggenschwiler et al., 2012), increasing the risk of resonant antenna effects. Regarding data quality, high-field acquisitions are likewise affected by increasingly stronger artifacts. EEG signals are particularly heavily degraded by magnetic induction effects, with previously less concerning environment noise sources, such as the He compression systems, exhibiting important contributions in recordings at 7T (Mullinger et al., 2008).

Reducing noise during acquisition is crucial to improve EEG data quality, especially at higher fields. This can be done by reducing the areas formed by electrode leads between each channel and the reference, thereby reducing magnetic induction effects. In this work, we assessed the importance of EEG cable length and geometry on noise sensitivity, at 7T, at the level of transmission between the cap and amplifiers. On a phantom model, the effects of different cable configurations were assessed, with specific attention to He coldhead contributions (study I). An optimized EEG setup with short bundled cables (approximately 12cm from cap to amplifiers) was implemented, and a series of safety tests were conducted, including EM simulations and surface temperature measurements on a phantom during fMRI acquisition (study II). Finally, the setup was employed for simultaneous EEG-fMRI acquisition on 5 healthy volunteers undergoing an eyes-open/eyes-closed task and a VEP run (study III).

Methods

Optimized EEG-fMRI setup

All measurements were performed on an actively-shielded Magnetom 7T head scanner (Siemens, Erlangen, Germany) equipped with a custom-built 8-channel Tx/Rx loop head array (Rapid Biomedical, Rimpar, Germany). For studies II and III, EEG data were recorded using two 32-channel BrainAmp MR plus amplifiers and a customized 64-electrode BrainCap MR model. The cap was designed with shortened leads terminating in two connectors at approximately 2cm from the cap surface. The cap connectors were linked to the EEG amplifiers via two 12cm bundled cables, with the amplifiers placed just outside the head RF array (Fig. 1).

After bandpass filtering (0.016 – 250Hz) and digitization (0.5μV), the EEG signals were transmitted to the control room via fiber optic cables. EEG sampling was performed at 5kHz, synchronized with the scanner clock. Abralyte gel was used to reduce electrode impedances. The scanner He coldheads were kept in function at all times in study II and study III.
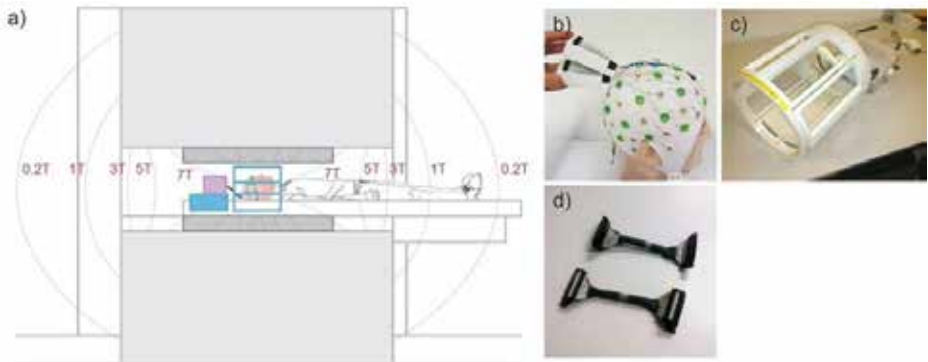

Figure 1. The optimized EEG-fMRI setup implemented in this work.

Study I – EEG cable noise contributions
This study assessed EEG noise sensitivity depending on the length and geometry of the ribbon cables connecting the cap to the amplifiers. EEG recordings were performed on a phantom, without MRI acquisition, both with and without the coldheads in function. Data were recorded using a single amplifier connected via a ribbon cable to an MR-compatible tester box, which was fixed to the phantom (to capture strictly cable-related noise contributions). Six cable configurations were tested, comprising 3 different lengths (100, 50, and 12cm) and 2 geometries: the typical flat ribbon configuration, and a bundled configuration where all channels are bunched together in a cylindrical shape (Fig. 1d).

Study II – safety testing
Here, a series of tests were performed to evaluate the impact of the optimized setup (12cm bundled configuration) on subject safety and EEG amplifier integrity. EM simulations were performed to study the effects on B1+ and SAR distributions across the head, as generated by the head RF array used in this work. The measurement was simulated in a realistic human model; EEG electrodes, gel, resistors, wire branches and connector positions were modeled according to the real cap. Temperature measurements were conducted on a phantom fitted with the EEG cap. Two probes were placed on electrodes AF8 and FT9, one in between

the EEG amplifiers, and another above the phantom, for reference. Temperature fluctuations were assessed during a 16min session comprising two fMRI runs: a sinusoidal GE-EPI sequence (69% of SAR limit) and a SE-EPI sequence (91% of SAR limit).

Study III – human acquisitions
Human tests intended to assess BOLD and EEG data quality using the optimized setup, particularly in terms of functional sensitivity. Five healthy volunteers underwent an eyes-open/eyes-closed run mediated by auditory cues, and a VEP run with reversing-checkerboard stimuli. After acquisition, EEG data underwent gradient and pulse artifact reduction (Allen et al., 2000; Niazy et al., 2005), downsampling, bad channel interpolation and re-referencing to the average reference. For the eyes-open/closed run, data were decomposed via ICA, and then reconstructed by manual selection of the relevant components. For the VEP run, data were first bandpass filtered to 4–30Hz, then ICA-decomposed, and finally reconstructed by selection of VEP-related components (Arrubla et al., 2013). FMRI data analysis comprised motion correction, slice-timing adjustments, brain segmentation, spatial smoothing (2mm) and temporal detrending (Smith et al., 2004). The datasets were then analyzed with a GLM approach (Worsley and Friston, 1995), modeling both paradigms as block designs.

Results

Study I – EEG cable noise contributions

Based on preliminary tests, the patient ventilation system was found to produce relevant noise contributions at frequencies below 30Hz, but could be switched off throughout all recordings (Nierhaus et al., 2013). With the He coldheads in function, using a 100cm conventional (flat) ribbon cable, most channels clearly displayed a stationary noise pattern of high frequency oscillations (> 20Hz), with a fundamental period of approximately 1s (Fig. 2a). A progressive increase in noise amplitude was clearly seen for channels running farther away from the reference, a trend which became greatly attenuated in the bundled geometry. Comparing all the tested cable configurations, the influence of cable length and geometry on noise power was found highly statistically significant, as was the impact of coldhead contributions ($p < 0.01$). Over all tested lengths, bundled cables yielded reductions of 0.2 – 69% in total noise power relative to flat cables, with the coldheads OFF, and 43 – 63% with the coldheads ON. Conversely, over the two geometry types, shortening from 100 to 12cm yielded reductions of 44 – 70% in noise power with the coldheads OFF, and 58 – 62% with the coldheads ON. Overall, the combination of cable bundling and shortening (from 100 to 12cm) led to a reduction of 84% in total noise power and of 91% in inter-channel noise power variability, with the coldheads in function (Fig. 2b).
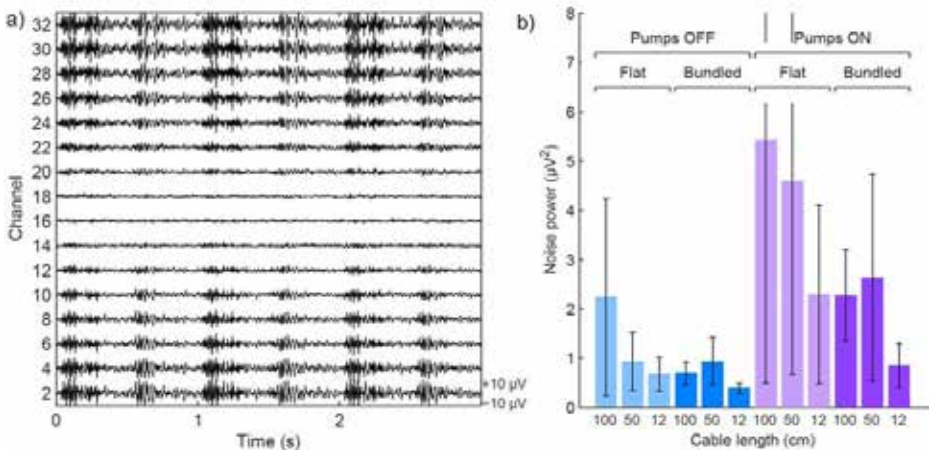

Figure 2. Left: EEG recordings using a 100cm flat ribbon cable, with the He coldheads in function. Right: average EEG noise power for different cable configurations, with and without the coldheads in function.

Study II – safety testing

In EM simulations, the presence of the EEG materials led to a general loss in B1+ amplitude of approximately 8.0%. The general field distribution was roughly maintained, but a number of local accentuated effects were observed in superior regions, mostly restricted to the scalp. SAR maps expressed similar trends, with an overall decrease of approximately 7.9%. A few local increases could be observed in superior-anterior regions, close to the skin, pushing the peak value from 0.39W/Kg to 0.43W/Kg with the cap. Regarding the temperature measurements, during the 16min session, temperature increases in either the reference probe or the two probes placed on EEG electrodes were found to be minimal (below 1°C). The sensor placed on the EEG amplifiers did measure stronger heating effects (from 21.4 to 27.9°C), although remaining well within their operating range.

Study III – human acquisitions

None of the volunteers reported any unusual skin heating effects, and the EEG amplifiers operated normally throughout all acquisitions. The ICA-reconstructed EEG data from the eyes-open/closed run revealed accentuated alpha modulation in occipital channels, with clear alpha power increases during most of the eyes-closed periods. In the fMRI data, significant negative BOLD signal changes were detected for eyes-closed periods in occipital regions, with average signal changes of -3.9% to -3.7%. For the VEP run, all subjects exhibited an average EEG response in occipital regions dominated by a positive peak occurring approximately 100ms after stimulus onset (Fig. 3a). This P100 peak reflected an anterior-posterior dipole, dominating the average GFP response at the same latency. On a single-trial scale, occipital responses were considerably noisier. Nevertheless, a trial-by-trial regression analysis showed that statistically significant responses ($p < 0.05$) were found in 164 – 177 trials out of 312 for this subject group. In the fMRI data, significant positive signal changes (+3.0% to +3.8%), correlated with checkerboard stimulation periods, were detected in occipital regions for all subjects (Fig. 3b).
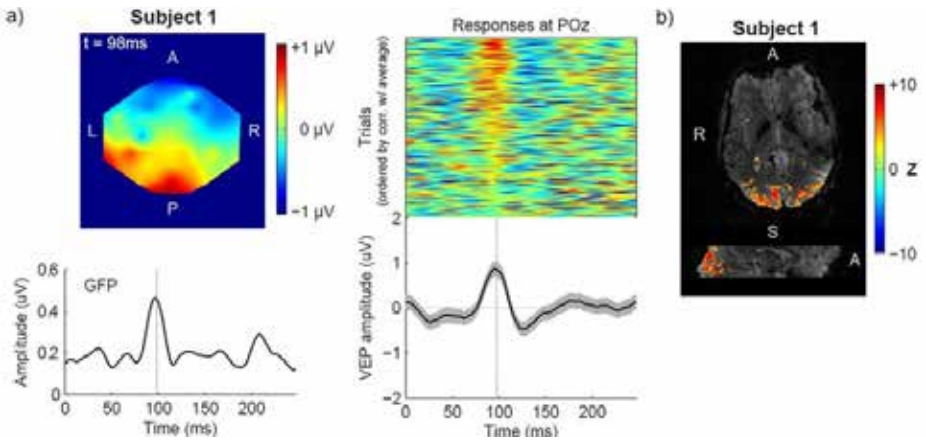
Figure 3. EEG (a) and fMRI (b) responses to the VEP run utilizing reversing-checkerboard stimulation.

Conclusion

The results obtained in this work demonstrate important benefits of careful optimization of the EEG signal chain for simultaneous EEG-fMRI. Focusing on the transmission stage between the cap and amplifiers, we have confirmed that both cable shortening and bundling effectively help reducing cable noise contributions to large extents. The optimized setup exhibited no significant safety concerns for subjects or amplifiers, the latter probably owing to the use of a Tx/Rx head array for more localized RF transmission. Based on human recordings, we conclude that alpha-wave modulation, VEPs and the concomitant BOLD signal changes can be detected with favorable sensitivity at 7T. Overall, setup improvements such as those here proposed, together with denoising approaches specifically tailored for simultaneous EEG-fMRI, steadily aid to bring this multimodal approach to satisfactory standards of signal quality, allowing for the full exploit of the benefits offered by high-field imaging.

References

[1] Allen, P.J., Josephs, O., Turner, R., 2000. A method for removing imaging artifact from continuous EEG recorded during functional MRI. Neuroimage 12, 230-239.

[2] Arrubla, J., Neuner, I., Hahn, D., Boers, F., Shah, N.J., 2013. Recording visual evoked potentials and auditory evoked P300 at 9.4T static magnetic field. PLoS One 8, e62915.

[3] Britz, J., Van De Ville, D., Michel, C.M., 2010. BOLD correlates of EEG topography reveal rapid resting-state network dynamics. Neuroimage 52, 1162-1170.

[4] Dempsey, M.F., Condon, B., 2001. Thermal injuries associated with MRI. Clin Radiol 56, 457-465.

[5] Eggenschwiler, F., Kober, T., Magill, A.W., Gruetter, R., Marques, J.P., 2012. SA2RAGE: a new sequence for fast B1+ -mapping. Magn Reson Med 67, 1609-1619.

[6] Gotman, J., Pittau, F., 2011. Combining EEG and fMRI in the study of epileptic discharges. Epilepsia 52 Suppl 4, 38-42.

[7] Mullinger, K., Brookes, M., Stevenson, C., Morgan, P., Bowtell, R., 2008. Exploring the feasibility of simultaneous electroencephalography/functional magnetic resonance imaging at 7 T. Magn Reson Imaging 26, 968-977.

[8] Neuner, I., Arrubla, J., Felder, J., Shah, N.J., 2013. Simultaneous EEG-fMRI acquisition at low, high and ultra-high magnetic fields up to 9.4T: Perspectives and challenges. Neuroimage.

[9] Niazy, R.K., Beckmann, C.F., Iannetti, G.D., Brady, J.M., Smith, S.M., 2005. Removal of FMRI environment artifacts from EEG data using optimal basis sets. Neuroimage 28, 720-737.

[10] Nierhaus, T., Gundlach, C., Goltz, D., Thiel, S.D., Pleger, B., Villringer, A., 2013. Internal ventilation system of MR scanners induces specific EEG artifact during simultaneous EEG-fMRI. Neuroimage 74, 70-76.

[11] Scheeringa, R., Fries, P., Petersson, K.M., Oostenveld, R., Grothe, I., Norris, D.G., Hagoort, P., Bastiaansen, M.C., 2011. Neuronal dynamics underlying high- and low-frequency EEG oscillations contribute independently to the human BOLD signal. Neuron 69, 572-583.

[12] Smith, S.M., Jenkinson, M., Woolrich, M.W., Beckmann, C.F., Behrens, T.E., Johansen-Berg, H., Bannister, P.R., De Luca, M., Drobnjak, I., Flitney, D.E., Niazy, R.K., Saunders, J., Vickers, J., Zhang, Y., De Stefano, N., Brady, J.M., Matthews, P.M., 2004. Advances in functional and structural MR image analysis and implementation as FSL. Neuroimage 23 Suppl 1, S208-219.

[13] van der Zwaag, W., Francis, S., Head, K., Peters, A., Gowland, P., Morris, P., Bowtell, R., 2009. fMRI at 1.5, 3 and 7 T: characterising BOLD signal changes. Neuroimage 47, 1425-1434.

[14] Worsley, K.J., Friston, K.J., 1995. Analysis of fMRI time-series revisited—again. Neuroimage 2, 173-181.

First Steps to Using Carbon Wire Loops to Correct for Artifacts in simultaneous EEG-fMRI

by Lars Hausfeld, PhD, Department of Cognitive Neuroscience, Maastricht University, Maastricht Brain Imaging Centre (M-BIC), The Netherlands

Abstract

The simultaneous acquisition of EEG and fMRI signals promises linked datasets with high temporal and spatial resolution, respectively. To make optimal use of the data from this advanced acquisition scheme, the attenuation of artifacts in EEG signals is necessary. One type of artifact that arises from blood pulsation, the so-called ballisto-cardiographic artifact, is difficult to correct for due to its variability. Here, a prototype BrainCap MR with carbon wire loops (CWLs) was used to directly measure this artifact while acquiring EEG and MRI data from one participant. Example data from two experimental paradigms show that signals from carbon wire loops can be used to efficiently regress these artifacts out and indicate the impact of such artifact attenuation for both event-related potential and stimulus reconstruction analyses.

Full Text

Electro-encephalography (EEG) was fundamental in advancing our understanding about brain processes and states in clinical and non-clinical populations and remains a tool of choice today given its precise temporal resolution, relatively low cost and portability. It is nowadays complemented with functional magnetic resonance imaging (fMRI), a technique that provides an increasingly precise spatial resolution that EEG source modelling cannot offer. During the last decade, studies have performed **simultaneous measurements of EEG and MRI** with the goal of combining the respective strengths of these techniques to better determine when and where neural processes occur at rest and in task contexts as well as in response to sensory stimuli. The strong magnetic field in the MRI scanner, however, induces noise in EEG measurements and proper correction methods are required before analyzing the EEG data. A first correction step for EEG signals is the removal of the MRI artifact related to gradient switching. While this artifact is of high amplitude, effective methods based on template subtraction have been introduced that are able to correct for this artifact (Allen et al., 2000; Niazy et al., 2005).

A different artifact arises from electrode motion due to blood pulsation, the ballisto-cardiographic (BCG) artifact. While this artifact's amplitude is small compared to the MRI scanning artifact – but still 3-4 times larger than EEG – it is difficult to correct for due to its spatio-temporal non-stationarity. Most preprocessing approaches make use of the simultaneously acquired electro-cardiogram (ECG) and advanced processing

(e.g., OBS-ICA; Debener et al., 2007). These techniques first detect occurrences of heart beats and subsequently correct for the BCG artifact by estimating the dynamic BCG artifact observed in EEG signals. In contrast, **a new approach not relying on the ECG uses carbon wire loops that are attached to the EEG cap to measure the BCG** (Abbott et al., 2015; van der Meer et al., 2016). Once measured, the BCG – and other motion-related artifacts apparent in additional measurements (e.g., from the He-pump or head movements) – can be removed by efficient regression-based approaches.

Here, I will share my experiences with first simultaneous EEG-fMRI measurements and analyses using a prototype BrainCap MR that included CWLs. In the best case, this provides a useful guidance for the (beginning of) cleaning EEG data from the BCG artifact. The correction methods used here were chosen to due to their availability as open-source EEGLAB toolboxes and straight-forward application.

The data were acquired in a 3T Siemens Prisma Fit MRI scanner at the Maastricht Brain Imaging Center (Maastricht, The Netherlands) from one participant. Throughout simultaneous EEG measurement, functional MRI data was acquired using a continuous EPI protocol (time-of-repetition [TR]: 1s, voxel size: 2x2x2.5mm3) that provided coverage of the temporal and large portions of the frontal lobe. The He-pump was not switched off during measurement. The participant was presented with three runs of an optimized MMN paradigm (Näätänen et al., 2004) and two repetitions of two 5-min audiobook excerpts. During each run of the oddball paradigm, the participant was presented with 495 standard tones and 240 deviants (opt1 sequence in Näätänen et al., 2004) and asked to focus on a fixation cross. The two audiobook excerpts were read by a female and male speaker and pauses between sentences or words were kept shorter than 300ms for analysis (Hausfeld et al., 2018).

EEG data was acquired with the prototype 32-channel BrainCap MR including an ECG electrode and additional channels for five carbon wire loops Data were recorded with a BrainAmp MR plus and BrainAmp ExG MR using BrainVision Recorder software (Brain Products GmbH, Gilching, Germany) with the recommended recording parameters for EEG-fMRI. The data was collected referenced to FCz.

EEG data were preprocessed in MATLAB (The Mathworks, Natwick, MA, version 9.5.0.944444, [R2018b]) using EEGlab (Delorme and Makeig, 2004, version 14.1.2) and additional toolboxes. First, the MRI gradient artifact was removed from EEG data using the FMRIB toolbox (version 1.21, http://fsl.fmrib.ox.ac.uk/eeglab/fmribplugin/; see Niazy et al., 2005). Here, I used the pop_fmrib_fastr.m function with the following parameters: a low-pass filter of 70Hz, 5-fold interpolation/upsampling (resulting in 25kHz signals), an averaging window size of 10 occurrences,

specification of the MRI trigger ('R128') and flags for volume triggers and not performing adaptive noise cancellation (default parameters otherwise).

```
EEG = pop_fmrib_fastr(EEG,70,5,10,'R128',0,0,0,0,0,0.03,32:37,'auto');
```

This resulted in a robust attenuation of the gradient artifact as can be seen from **Figure 1A that shows both corrected EEG as well as CWL time-courses**. Channels P4, TP10 and POz (not presented here) showed abnormal EEG signals and were interpolated after the CWL-based correction.
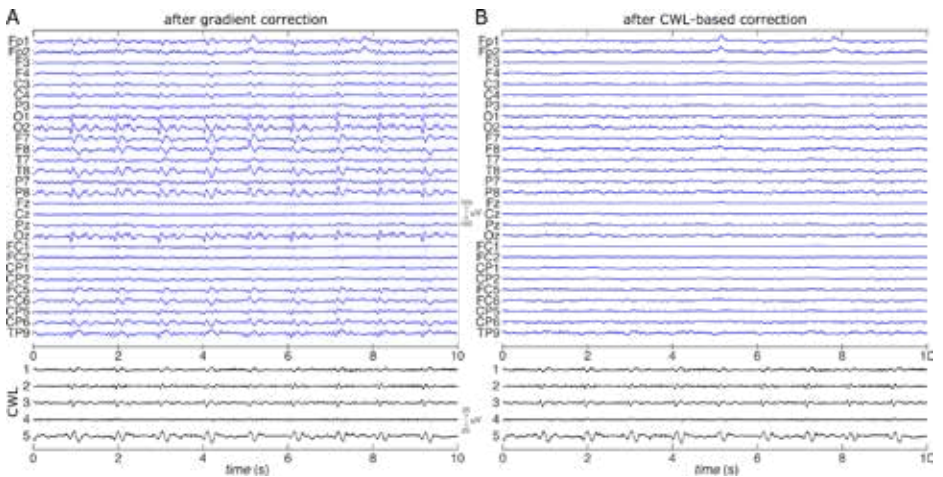
Figure 1. Example EEG and CWL signal traces before and after CWL-based correction. A) The upper panel shows 10-s example EEG traces from the different electrodes. In the lower panel, the CWL traces are presented. Note the clear heart-beat related artifacts at about 60bpm in CWLs. The EEG recordings show the large impact that the BCG artifact has on electrodes. B) Same as in A) but after CWL-based correction. Note here the very strong attenuation for the BCG artifact observed in A) as well as the eye blinks at Fp1/Fp2.

Unfortunately, the ECG signal time-course showed aberrant signals during this MRI acquisition (without MRI acquisition, typical ECG patterns were obtained). **Distortion of the ECG signal inside the scanner can occur** and occasionally the signal can be unusable. However, the preprocessing of EEG and removal of the BCG based on CWL measurements does not rely on ECG recordings and thus could be performed. In contrast, other approaches (Debener et al., 2007; Niazy et al., 2005) to attenuate BCG artifacts require temporal information on the heartbeat occurrences (QRS complex) extracted by a robust detection algorithm and manual or semi-automated setting/correction of these triggers (e.g., BrainVision Analyzer 2, FMRIB toolbox). If present, **CWL signals could be used as alternative signals for detecting heartbeat events** when necessary, especially when facing distorted ECG recordings.

After downsampling of the EEG and CWL data to 500Hz, the BCG and other potential motion artifacts were corrected by using the cwleegfmri toolbox (http://sccn.ucsd.edu/eeglab/plugins/CWRegrTool.zip; van der Meer et al., 2016). More specifically, this approach creates windowed regressors from CWL time-courses that are used to regress out – channel-by-channel – the signal traces that are related to the CWL signals. As these do not measure any EEG but motion-induced currents amongst which the BCG artifact but also other potential motion artifacts, this step corrects for these non-brain signals (it has been suggested that residuals of gradient artifacts might also be attenuated as these will be present in the CWL signals as well, Abbott et al., 2015). The function pop_cwregrssion.m was called with mainly default parameters specifying the sampling rate (500Hz), window duration (4s), delay (0.021s), tapering factor (1), tapering function ('hann'), channel indices of carbon wire loops, channel indices of EEG, and the regression approach ('taperedhann'):

```
EEG = pop_cwregression(EEG,500,4,0.021,1,'hann',33:37,1:31,'taperedhann',0);
```

The result of this correction can be seen in **Figure 1B that shows the CWL-corrected data and showcases the attenuation of the BCG artifact**. Please note the residual BCG – though small – that remained after correction (e.g., in channels Oz or TP9) and that further optimization of regression parameters might lead to increased attenuation of the BCG artifact. Furthermore, it becomes clear that eye-related artifacts remain in the corrected dataset (here at 5s and 8s most prominent in channels Fp1 and Fp2). These can now be effectively corrected for by a method of choice. From this point onwards, researchers should be able to follow their desired preprocessing and analysis scheme. For these two datasets, I chose to use Independent Component Analysis (ICA) to decompose and further process the CWL-corrected EEG data and remove independent components (ICs) that represented blinks and eye-movements.

To gain quantitative insight into the artifact handling using the CWL signals, Figure 2 presents a coarse metric that indicates the strong attenuation of the BCG artifact and other motion artifacts as picked up by the CWLs. While the time course of EEG channels showed a high correlation between CWL and EEG signals of $|r| = 0.15$ for most channels, the highest correlation after CWL-based correction among all channels was $|r| = 0.021$ and $|r| = 0.041$ for the MMN and audiobook dataset, respectively. For ICs that were computed separately on data with and without CWL-based correction one can observe a similar effect with the maximally correlated component of the CWL-corrected dataset at $|r| = 0.026$ and $|r| = 0.047$ while only 5 and 4 components remained below this value when performing ICA on the dataset without CWL signals regressed out. While this was only observed with two datasets of one participant, it suggests an advantage of the CWL-based correction over using ICA only: a few independent components were highly correlated ($|r| > 0.2$) with the CWL signals and would be chosen as "BCG-components" to be removed. However, most other components also showed a high similarity with CWL signals (i.e., motion-related artifacts) that would remain in the corrected data.

A comparison with the OBS or OBS-ICA approach (Debener et al., 2007; Niazy et al., 2005) was unfortunately not possible due to the poor quality of the ECG signal (see above). However, **in terms of computational effort, the CWL approach is faster and was in my experience less sensitive to changes of parameters.**
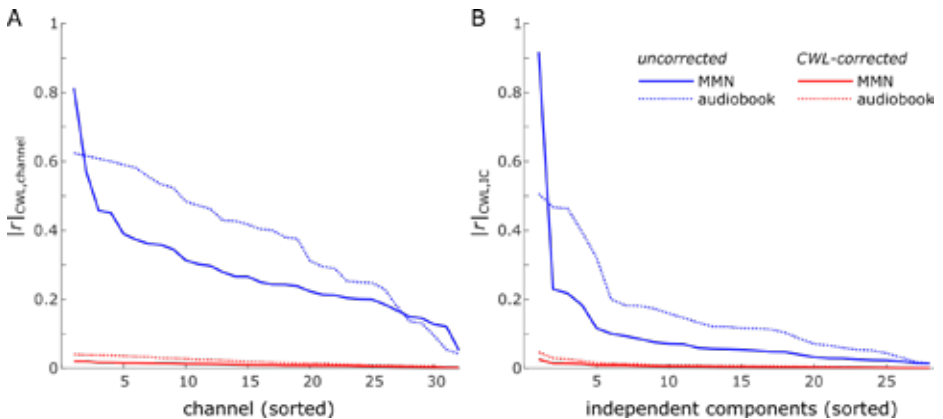
Figure 2. Similarity of CWL and EEG signals before and after CWL-based correction. A) As an indication of artifacts detected by CWLs in the acquired EEG data, the 5 CWL signals were correlated with signals from EEG channels. For simplicity only the highest absolute correlation is presented here. Blue lines show the similarity of EEG and CWL signals for uncorrected data, red lines show the similarity for data after CWL regression. Solid (MMN) and dotted lines (audiobook) indicate the two sets of experimental data.

When analysing the data acquired during the oddball paradigm, ERPs computed from the dataset without CWL-based artifact correction look noisy – in particular for deviants relying on less trials – with some typical ERP components being identifiable (Figure 1A). In contrast, the data after regressing out CWL signals showed cleaner ERPs with typical components clearly discernible (Figure 1B). **Please keep in mind that this is data from a single participant;** in usual studies grand average ERPs are computed from 20+ participants.
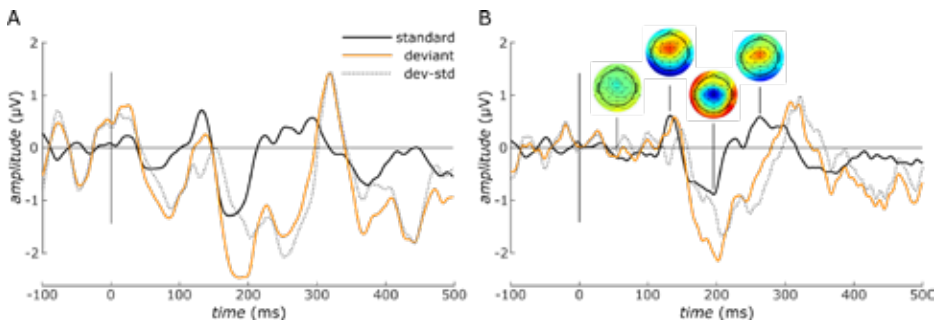

Figure 3. ERPs from the MMN paradigm before and after CWL-based correction. A) Solid lines show the recorded ERPs for a fronto-central electrode cluster (Fz, FCz, Cz, FC1, and FC2) for the standard (black) and deviant (orange), the dotted grey line presented the difference deviant – standard before CWL-based correction. B) same as in A) but for after the CWL signal were regressed out. In addition, topographic plots are presented at selected latencies. These show typical auditory evoked patterns with fronto-central vs lateral polarity inversion.

In a final step, the data acquired during audiobook presentation was analyzed with a stimulus reconstruction approach that estimates so-called multivariate temporal response functions (mTRFs). In short, using the continuously acquired EEG data, part of the data was selected to train an mTRF model using the MATLAB-based mTRF toolbox (Crosse et al., 2016). After training, this model was applied to unseen test data to reconstruct the speech envelope presented while this unseen data was acquired. The predicted and the actual envelope are then compared using the correlation coefficient. For this single-participant dataset, the stimulus could be reconstructed well with rmTRF = 0.116 for the CWL-corrected data. This is in the higher range of reconstruction performances in comparison to a previous EEG-fMRI study (Puschmann et al., 2017). Perhaps surprising, the reconstruction for the dataset without CWL-based correction showed a higher reconstruction of rmTRF = 0.136. I speculate that this is due to the high sensitivity of the mTRF models, which are susceptible to exploiting artifacts (here: BCG); this exemplifies that thorough cleaning of EEG data **will provide researchers with more confidence that their results reflect neural processing**, which

is even more important in the EEG-hostile environment of the MRI scanner.

To conclude, **carbon wire loop signals can substantially aid the cleaning of EEG datasets obtained during fMRI data acquisition**. As these loops measure the artifact related to blood pulsation and other motion sources directly at the level of EEG channels, a fast regression algorithm is able to attenuate these artifacts substantially, which would require more advanced approaches otherwise. Unfortunately, a direct comparison with these techniques was not possible but previous results suggest added benefits from CWL signals in comparison to other approaches (Abbott et al., 2015; van der Meer et al., 2016). Taken together, the fast and intuitive use and artifact measurements close to EEG channels make CWLs a powerful tool for cleaning EEG data obtained from simultaneous EEG-fMRI measurements.

References

Abbott DF, Masterton RAJ, Archer JS, Fleming SW, Warren AEL, Jackson GD. 2015.
Constructing Carbon Fiber Motion-Detection Loops for Simultaneous EEG-fMRI.
Front Neurol 5:260. doi:10.3389/fneur.2014.00260

Allen PJ, Josephs O, Turner R. 2000.
A Method for Removing Imaging Artifact from Continuous EEG Recorded during Functional MRI.
Neuroimage 12:230–239. doi:10.1006/nimg.2000.0599

Crosse MJ, Di Liberto GM, Bednar A, Lalor EC. 2016.
The Multivariate Temporal Response Function (mTRF) Toolbox: A MATLAB Toolbox for Relating Neural Signals to Continuous Stimuli.
Front Hum Neurosci 10:604. doi:10.3389/fnhum.2016.00604

Debener S, Strobel A, Sorger B, Peters J, Kranczioch C, Engel AK, Goebel R. 2007.
Improved quality of auditory event-related potentials recorded simultaneously with 3-T fMRI: Removal of the ballistocardiogram artefact.
Neuroimage 34:587–597. doi:10.1016/j.neuroimage.2006.09.031

Delorme A, Makeig S. 2004.
EEGLAB: an open source toolbox for analysis of single-trial EEG dynamics including independent component analysis.
J Neurosci Methods 134:9–21. doi:10.1016/j.jneumeth.2003.10.009

Hausfeld L, Riecke L, Valente G, Formisano E. 2018.
Cortical tracking of multiple streams outside the focus of attention in naturalistic auditory scenes.
Neuroimage 181:617–626. doi:10.1016/j.neuroimage.2018.07.052

Moosmann M, Schönfelder VH, Specht K, Scheeringa R, Nordby H, Hugdahl K. 2009.
Realignment parameter-informed artefact correction for simultaneous EEG-fMRI recordings.
doi:10.1016/j.neuroimage.2009.01.024

Näätänen R, Pakarinen S, Rinne T, Takegata R. 2004.
The mismatch negativity (MMN): towards the optimal paradigm.
Clin Neurophysiol 115:140–144. doi:10.1016/j.clinph.2003.04.001

Niazy RK, Beckmann CF, Iannetti GD, Brady JM, Smith SM. 2005.
Removal of FMRI environment artifacts from EEG data using optimal basis sets.
Neuroimage 28:720–737. doi:10.1016/j.neuroimage.2005.06.067

Puschmann S, Steinkamp S, Gillich I, Mirkovic B, Debener S, Thiel CM. 2017.
The Right Temporoparietal Junction Supports Speech Tracking During Selective Listening: Evidence from Concurrent EEG-fMRI.
J Neurosci 37:11505–11516. doi:10.1523/JNEUROSCI.1007-17.2017

van der Meer JN, Pampel A, Van Someren EJW, Ramautar JR, van der Werf YD, Gomez-Herrero G, Lepsien J, Hellrung L, Hinrichs H, Möller HE, Walter M. 2016.
Carbon-wire loop based artifact correction outperforms post-processing EEG/fMRI corrections—A validation of a real-time simultaneous EEG/fMRI correction method.
Neuroimage 125:880–894. doi:10.1016/j.neuroimage.2015.10.064

Multimodal Fingerprints of Resting State Networks as assessed by Simultaneous Trimodal MR-PET-EEG-Imaging

by Shah NJ[1,2,3,4,5], Rajkumar R[1,3,6], Neuner I[1,3,6]*

[1]Institute of Neuroscience and Medicine 4, INM-4, Forschungszentrum Jülich, Germany

[2]Institute of Neuroscience and Medicine 11, INM-11, Forschungszentrum Jülich, Germany

[3]JARA – BRAIN – Translational Medicine, Germany

[4]Department of Neurology, RWTH Aachen University, Germany

[5]Monash Biomedical Imaging, School of Psychological Sciences, Monash University, Melbourne, Victoria, Australia.

[6]Department of Psychiatry, Psychotherapy and Psychosomatics, RWTH Aachen University, Germany

*corresponding author: Professor Dr. Irene Neuner, Institute for Neuroscience and Medicine 4, INM4, Forschungszentrum Jülich GmbH, 52425 Jülich, Germany (i.neuner@fz-juelich.de, phone +49 2461 616356, fax +49 2461 611919

Short abstract

Recent efforts have seen advances in hybrid imaging, i.e. simultaneous acquisition of data from magnetic resonance imaging – electroencephalography (MRI-EEG) (Mullinger et al. 2011; Neuner et al. 2013) or MRIpositron emission tomography (PET) (Wehrl et al. 2013; Shah et al. 2013). In this work, we show the implementation of simultaneous trimodal imaging by employing the benefits of EEG, to acquire the electrophysiology of the brain, simultaneously with PET, to ascertain metabolic details, and MRI, to integrate brain function and structure. Trimodal imaging methodology is presented here for the first time, and we have carried out a pilot study to highlight its advantages. This article is based on recently published work, Shah NJ, Arrubla J, Rajkumar R, Farrher E, Mauler J, Kops ER, et al. Multimodal Fingerprints of Resting State Networks as assessed by Simultaneous Trimodal MR-PET-EEG Imaging. Scientific Reports 2017;7:6452. doi:10.1038/s41598-017-05484-w.

Introduction

The human brain is one of the most complex and efficient organs in the body. It can be functionally segregated into various functional networks (Shirer et al. 2012). One such functional network is the resting state network (RSN), which organises the brain in a large-scale cerebral network, in the absence of any external stimulation (Biswal et al. 1995). Among RSNs, the so called default mode network (DMN) is widely studied and its hubs are found to be most vulnerable to neurological disorders (Chételat & Marine 2013). It has also been found that the functional connectivity within DMN has a high impact on task performance (Berkovich-Ohana et al. 2016). The energy metabolism of the DMN and its relationship with the concentration of the neurotransmitters, as well as ist electrophysiological signatures, could be potential biomarkers in the early detection of neuro-disorders. To date, such parameters have been studied using neuroimaging techniques via sequential

measurements. However, sequential measurement has the major confounding factor that the data are recorded at different time points and the physiological condition of the brain might have altered between the different time points. Also, from a clinical routine point of view, sequential tomography (PET) and electrophysiological information via electroencephalography (EEG), the modalities of MRI, PET and EEG have been combined into a single trimodal imaging facility in our Institute. The simultaneous trimodal facility provides high spatial resolution MR images, highly
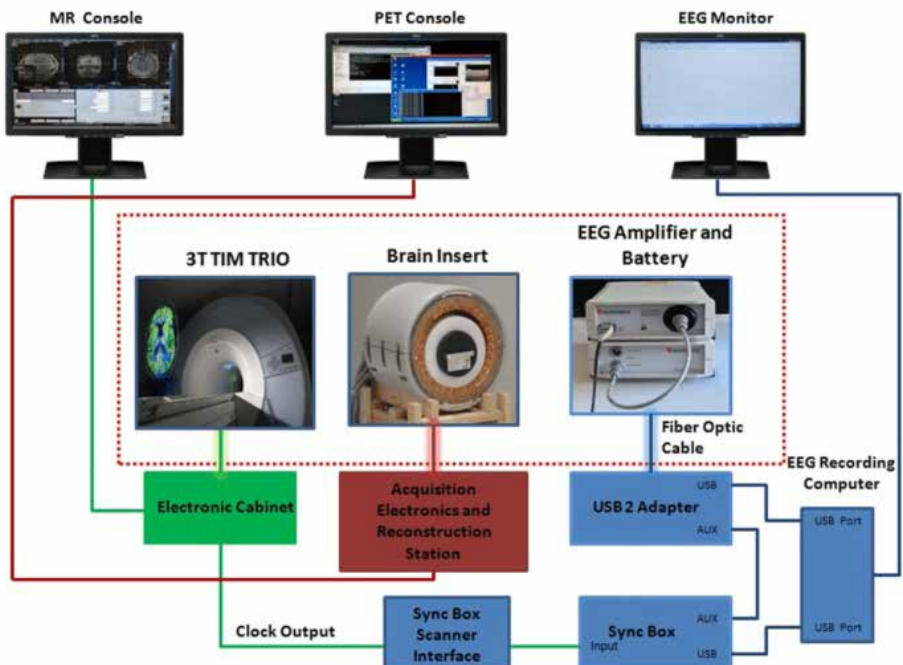
Figure 1: Trimodal set-up. The diagram displays the connections between the various components of the simultaneous MR-PET-EEG setup. The components inside the red dotted, rectangular box are inside the RF-shielded MR room. (Shah NJ, et. al., 2017)

measurement is time consuming and requires more human resources. Thus, in order to simultaneously measure structural and functional information via magnetic resonance imaging (MRI), metabolic information via positron emission molecular specific PET images (depending on the radiolabelled tracer used) and high temporal resolution EEG signals. By utilising the complementary information provided by each modality in this novel imaging facility, we investigated the DMN region of the brain

and characterised DMN in healthy male subjects using multimodal fingerprints, such as functional connectivity via fMRI, energy metabolism via 2- [18F]fluoro-2-desoxy-D-glucose PET (FDG-PET), mean diffusivity (MD) via diffusion weighted imaging (DWI), the inhibition – excitation balance of neuronal activation via MR spectroscopy (MRS), and electrophysiological signature via EEG.

Methods

Data Acquisition

In a single imaging session per subject, MRI, FDG-PET and EEG data were recorded simultaneously from 11 healthy male volunteers (age 28.6 ± 3.4) using a 3T hybrid MR-BrainPET system (Siemens, Erlangen, Germany). A 32-channel, MR-compatible EEG system from Brain Products GmbH (Gilching, Germany) was used for EEG data acquisition. The trimodal data acquisition is shown in Fig. 1.

The subjects were instructed to fast overnight and to skip breakfast on the day of measurement. First, the subjects were prepared for EEG recording. An intravenous (IV) line was inserted in the right arm of the subject to facilitate injection of the FDG tracer. FDG tracer (~200 MBq) was injected as a single bolus into the subject, while lying in supine position in the scanner. Dynamic PET data recording in list mode started immediately after the injection of the tracer and lasted 60 minutes. Simultaneously, MR structural data and MRS data (in posterior cingulate cortex (PCC), medial prefrontal cortex (MPfC), and precuneus) were recorded. Exactly 50 minutes after the FDG tracer injection, eyes closed resting state fMRI (T2*-weighted echo planar imaging) was measured for about 6 minutes. Simultaneously during resting state fMRI, the EEG data were also recorded using BrainVision Recorder (Brain Products GmbH, Gilching, Germany).

Data Analysis

MRS: The GABA ratio (to Cr+PCr) and the glutamate-glutamine ratio (to Cr+PCr) were extracted for each of the three investigated voxels (PCC, MPfC and precuneus) and used for posterior analyses.

fMRI: Data was pre-processed for motion correction, brain extraction, spatial smoothing (6 mm FWHM) and high pass filtering (100 s). DMN regions were identified for every subject via temporal concatenation ICA. A group DMN mask was created using the mean of the identified DMN regions in each subject. Similarly, a non-DMN mask was created by subtracting the DMN mask from the whole brain mask. Additionally, for functional network level comparison, a mask of the dorsal DMN (dDMN) and the sensorimotor network (SMN) was obtained from the 90 fROI atlas (Shirer et al. 2012). All four masks (DMN, non-DMN, dDMN and SMN) were corrected for grey matter. After pre-processing and intensity normalisation (grand mean scaling), the mean BOLD signal intensity was extracted individually from the created masks for each subject.

DWI: Diffusion data were corrected for eddy-current and motion distortions. The MD maps (Basser & Pierpaoli 1996) were calculated for

further analysis.

PET: PET data reconstructed between 30 and 60 minutes after the injection of the FDG tracer was used for the analysis. The PET images were converted to standard uptake value (SUV) maps, accounting for the body weight and injected dose of every subject.

EEG: EEG data were partly pre-processed using a BrainVision Analyzer 2 (Brain Products, Germany). The EEG raw data were corrected for artefacts (gradient, ocular, cardioballistic). The de-noised data was exported to the LORETA-KEY software. The distribution of the neuro-electrical generators was computed using eLORETA (Pascual-Marqui et al. 1994) at different EEG frequency bands (δ, θ, α and β).

The mean MD, SUV and neuro-electrical generators (from eLORETA) values were extracted from the created masks. A Wilcoxon-Mann-Whitney (WMW) exact test was performed using the SAS software (version 9.4) to compare the mean value of each parameter in the DMN and the non-DMN, as well as in the dDMN and the SMN. Additionally, bivariate correlation tests were performed between calculated parameters using the Spearman rankorder correlation coefficient.

Results

fMRI: The WMW test showed that the mean BOLD signal in the DMN mask was higher than outside the DMN mask ($Z = 3.94$, two sided $p < 0.001$). Similarly the mean BOLD signal in

the dDMN mask was higher than in the SMN mask ($Z = 3.94$, two sided $p < 0.0001$).

DWI: No significant differences were found between the mean MD in the DMN and in non DMN ($Z = 1.44$, two sided $p = 0.15$) as well as in dDMN mask and in SMN mask ($Z = 0.06$, two sided $p = 0.95$)

PET: The WMW test showed that the SUV in the DMN mask was higher than outside the DMN mask ($Z = 3.94$, $p < 0.0001$). Similarly, the SUV in the dDMN mask and in SMN mask ($Z = 3.81$, two sided $p < 0.0001$) showed a significant difference.

EEG: The WMW test showed a significant difference in the electrical sources between the DMN and SMN in δ ($Z = 3.35$, two sided $p = 0.0003$), θ ($Z = 3.22$, two sided $p = 0.0006$), α ($Z = 3.09$, two sided $p = 0.001$) and $\beta-1$ ($Z = 2.76$, two sided $p \leq 0.0041$) frequency bands. Such differences were not found in the $\beta-2$ ($Z = 0.2$, two sided $p = 0.85$) and $\beta-3$ ($Z = 0.98$, two sided $p = 0.33$) frequency bands.

The Spearman rank-order correlation did not show any statistically significant correlation between the MRS parameters (the GABA ratio and the glutamate-glutamine ratio) and any of the other measured imaging parameters, such as BOLD intensity, MD, SUV and electrical generators.

The Spearman rank-order correlation shows a statistically significant positive correlation between BOLD signal intensity and SUV of FDG in DMN ($rs = 0.77$, $n = 11$, $p = 0.0053$) and

dDMN (rs = 0.71, n = 11, p = 0.0146) (Fig. 2).

Discussion and Concludions

Our aim of simultaneously measuring MRI, PET and EEG was successfully developed and implemented for the first time. This exploratory study, using FDG as PET tracer for the trimodal study, has demonstrated the feasibility of measuring three modalities simultaneously. Also, the significant differences observed in

for δ ,θ, α and β-1. These frequency ranges play an important role in the long-range synchronisation for the effective coupling between more remote brain regions (Uhlhaas & Singer 2015).

This explorative pilot study in humans has the limitations of being based only on a small sample size and on the limited number of parameters assessed. However, the
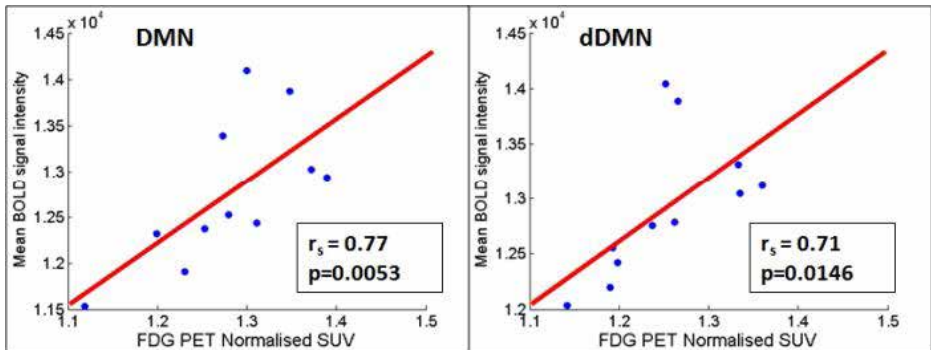

Figure 2: Correlation plot between normalised SUV uptake of FDG PET and BOLD signal intensity in DMN (right side) and dDMN (left side). (Shah NJ, et. al., 2017)

calculated parameters (BOLD intensity, SUV, electrical generators) between DMN and non-DMN regions during resting state confirm the reliability of the results.

Higher correlation between resting state BOLD intensity and metabolic activity of glucose (accessed via FDGPET) in the DMN shows that higher neuronal activation is coupled to a higher energy consumption, which is in agreement with a study by Riedl et al. (Riedl et al. 2014). A significant difference was found between the DMN and SMN when comparing the electrical sources

successful implementation of the trimodal simultaneous approach is demonstrated here in a general context.

In addition to providing insight into basic neuroscience questions addressing neurovascular-metabolic coupling, this trimodal methodology lays the foundation for investigating individual physiological and pathological fingerprints/biomarkers. These then have the potential for supporting a wide research field addressing, for example, healthy aging, gender effects, plasticity and various diseases. In particular, studies

addressing pharmacological challenges will profit from this approach which paves the way for the possibility to predict individual treatment response in the framework of individually tailored medication. This would have significant benefits for the treatment of psychiatric and neurological disorders ranging from major depression and schizophrenia to epilepsy and neurodegenerative diseases.

Acknowledgements

References

[1] Basser, P.J. & Pierpaoli, C., 1996. Microstructural and Physiological Features of Tissues Elucidated by Quantitative-Diffusion-Tensor MRI. J. Magn. Reson., Ser. B, 111, pp.209–219.

[2] Berkovich-Ohana, A. et al., 2016. Data for default network reduced functional connectivity in meditators, negatively correlated with meditation expertise. Data in Brief, 8, pp.910–914.

[3] Biswal, B. et al., 1995. Functional connectivity in the motor cortex of resting human brain using echo-planar MRI. Magnetic resonance in medicine, 34(4), pp.537–41.

[4] Chételat, G. & Marine, 2013. Neuroimaging biomarkers for Alzheimer's disease in asymptomatic APOE4 carriers. Revue Neurologique, 169(10), pp.729–36.

[5] Mullinger, K.J., Yan, W.X. & Bowtell, R., 2011. Reducing the gradient artefact in simultaneous EEG-fMRI by adjusting the subject's axial position. NeuroImage.

[6] Neuner, I. et al., 2013. Simultaneous EEG-fMRI acquisition at low, high and ultra-high magnetic fields up to 9.4T: Perspectives and challenges. NeuroImage.

[7] Pascual-Marqui, R.D. et al., 1994. Low resolution electromagnetic tomography: a new method for localizing electrical activity in the brain. Int J Psychophysiol, 18(1), pp.49–65.

[8] Riedl, V. et al., 2014. Local activity determines functional connectivity in the resting human brain: a simultaneous FDG-PET/fMRI study. J Neurosci, 34(18), pp.6260–6.

[9] Shah, N.J. et al., 2013. Advances in multimodal neuroimaging: Hybrid MR-PET and MR-PETEEG at 3 T and 9.4 T. J Magn Reson, 229, pp.101–15.

[10] Shirer WR, Ryali S, Rykhlevskaia E, Menon V, Greicius MD, 2012. Decoding subject-driven cognitive states with whole-brain connectivity patterns. Cereb. cortex, 22(1), pp.158–165.

[11] Uhlhaas, P.J. & Singer, W., 2015. Oscillations and neuronal dynamics in schizophrenia: The search for basic symptoms and translational opportunities. Biol. Psychiatry, 77(12), pp.1001–1009.

[12] Wehrl, H.F. et al., 2013. Simultaneous PET-MRI reveals brain function in activated and resting state on metabolic , hemodynamic and multiple temporal scales. Nature Medicine, 19(9), pp.1184– 1189.

Support Tip
Safety Tips for our new EEG-fMRI solutions

by Dr. Tracy Warbrick, Application Specialist EEG-fMRI (Brain Products)

In this article we provide an overview of our EEG-fMRI safety recommendations especially with respect to our recent developments. We will consider our sequence guidelines and what limits apply to our various caps. We will also provide an overview of recommendations for setting up the system in the scanner. Recommendations for sources of further information will also be made throughout.

Background

The BrainAmp MR (plus) system has benefited from some updates in the past few years. Specifically, we have updated the design of BrainCap MR to improve safety, introduced new, more flexible sequence guidelines, introduced carbon wire loops (CWLs) to help with handling motion artifact, and in this issue of our newsletter we are proud to announce the release of the R-Net MR and the CWL regression transformation in BrainVision Analyzer 2.2.2 (and later).

We take safety very seriously for EEG-fMRI because the EEG system is vulnerable to the effects of the MR environment. The EEG system is a recording circuit (EEG electrode versus reference electrode) and consists of electrodes, lead wires, and an amplifier. We place this system inside a static magnetic field, and during scanning we use strong switching gradient fields and radio frequency (RF) pulses. The EEG-system is susceptible to heating due to RF-coupling as well as eddy currents. This has consequences for the function of equipment and the wellbeing of the participant. As such, we provide recommendations for how to use the BrainAmp MR systems safely in the MR environment at 3 T.

We strive to keep our products and guidelines up to date and when we revise any of our documentation, we make it available for free on our website; **please be sure to check for current versions so you always have the most recent information.**

Let's start with our sequence guidelines

We introduced the B1+rms thresholds in 2020. We've always had limitations for acceptable MRI sequences to restrict the amount RF exposure of the EEG system, but previously they were a little more restrictive and not so easy to adapt to advanced fMRI sequences. We wanted to make the guidelines more flexible and allow researchers to use advanced fMRI sequences, e.g. MB fMRI, so we introduce the **B1+rms threshold**. Further information on B1+rms can be found in this article.

Keep in mind that the system is intended for simultaneous EEG-fMRI measurements, as such we have fMRI BOLD imaging in mind when testing and setting the limits. The

B1+rms limit might also allow other, non-fMRI sequences, to be used but there will also be sequences that are outside of these guidelines. We appreciate that researchers might want to use sequences with a higher RF load, e.g. turbo spin echo sequences, arterial spin labelling, or even fMRI sequences with a high RF load, but this is not possible if the B1+rms is above the threshold. The potential **consequences for using sequences that are outside the guidelines are damage to the EEG equipment or injury to the participant** due to heating of components of the EEG system. We would like to avoid these consequences; therefore, we provide guidelines on how to use the EEG system safely.

B1+rms in practice

Since introducing the B1+rms limits we've had some questions from our users on how to determine B1+rms and where to find it. Specific sequence parameters are outside of our expertise so we are unable to comment on which values you should use. Also, the exact parameters to change to manipulate B1+rms for a given sequence will vary across scanners. However, we can offer a few tips on how to use B1+rms.

Tip: *The parameters that influence the B1+rms of a sequence are similar to those we consider in relation to reducing specific absorption rate (SAR), for example flip angle, RF pulse duration, number of slices in a given repetition time (TR). Your scanner operator should be able to help you adjust the relevant parameters in your MRI sequence*

Tip: T*he location of the B1+rms display on the scanner console is different for each manufacturer, however, it is likely to be close to where the SAR parameters are displayed*

Note that on Siemens' systems there is a 'predicted' and a 'current' B1+rms. The 'predicted' value should be used to determine the B1+rms of the sequence you would like to use.

What B1+rms threshold applies to your setup?

In 2020 we also made some modifications **to the standard BrainCap MR**: shorter cable tree, increased resistance on drop-down leads (e.g. ECG lead), and the introduction of a shorter (10 cm) bundled cable to connect the EEG cap to the amplifier. The updated features of the new design allowed the BrainCap rev. 3 to be tested with stronger MRI sequences. The R-Net MR has same safety features as the BrainCap MR rev. 3.

Our current standard setup includes the BrainCap MR rev. 3 or the R-Net MR used with a 10 cm bundled connection cable. The B1+rms threshold for this standard setup is 1.5 µT. However, we know that some labs have older caps or prefer to use the longer (30 cm) connection cable due to their local setup. Don't worry, you can continue to use your existing BrainCap MRs but note that the B1+rms threshold is more restrictive (1.0 µT) and is in line with our previous recommendations for the BrainCap MR. Figure 1 provides an overview of what B1+rms

threshold applies to different combinations of caps and connection cable lengths. **All connection cables longer than 30 cm (e.g. 100 cm) are intended only for the cap preparation outside the magnet room**. These cables should never be part of a recording setup inside the scanner room.

Note that adding carbon wire loops doesn't change the B1+rms threshold for the BrainCap MR or R-Net MR.

Tip: *For older caps, we recommend replacing the 30 cm ribbon cable that connects the cap to the amplifier with a 10 cm bundled cable.*

This doesn't reduce the overall length as much as for the new BrainCap MR, or change the B1+rms threshold, but it will help with finding a better position for the BrainAmp MR (plus) inside the scanner bore.

Tip: How do I know what threshold applies to my cap?
If the **cable tree** of your BrainCap MR is longer than 31 cm it is an older (or customized) BrainCap MR.
To be sure whether your BrainCap MR is a rev. 3 you should check the **document delivered with your cap** which provides the layout and specification.
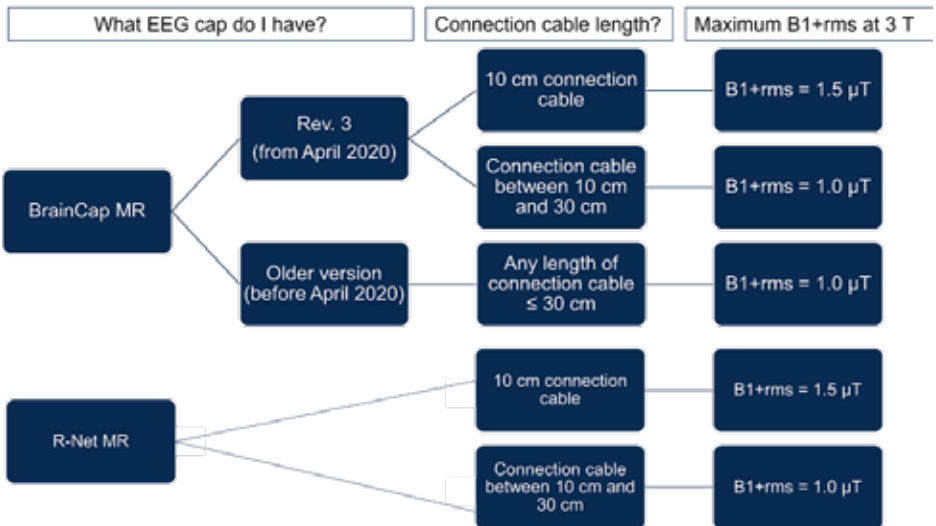
*Figure 1. Overview of the B1+rms threshold that should be used for different combinations of EEG caps and connection cables. Note that by connection cable, we mean the cable that connects the BrainCap MR or R-Net MR to the BrainAmp MR (plus). Note that connection cables longer than 30 cm are intended for cap preparation outside of the scanner room and are not intended to be part of the set up inside the scanner.*

Setting up the system in the bore

In addition to staying within the sequence guidelines you should also follow our placement recommendations for setting up the BrainAmp MR (plus) system inside the scanner. The exact setup can be dependent on local factors such as the type of scanner you have, the head coil that you plan to use, and whether you have any other equipment inside the scanner bore. But there are some **basic principles that should always be followed**. Figure 2 illustrates a recommended setup and lists the key points to consider when setting up your BrainAmp MR (plus) system.

Conclusion

We have provided a refresher on the main safety considerations for setting up your EEG-fMRI study and how these recommendations apply to our new solutions. If you would like to learn more about how to setup your BrainAmp MR (plus) system safely you can watch the recording of our recent webinar "Getting ready for simultaneous EEG-fMRI: safety and setup basics" that is available on our Brain Products Academy webinar channel.

In this article we have covered setting up EEG measurements, for information on using the BrainAmp ExG MR for peripheral physiology measurements please refer to our series of support tips on ExG-fMRI measurements, the first of which covered EMG-fMRI and can be found here. If you have any questions about setting up your BrainAmp MR system please contact our Technical Support team and if you would like more information on our new solutions please contact contact us (via email, contact form or chat) or your local distributor.
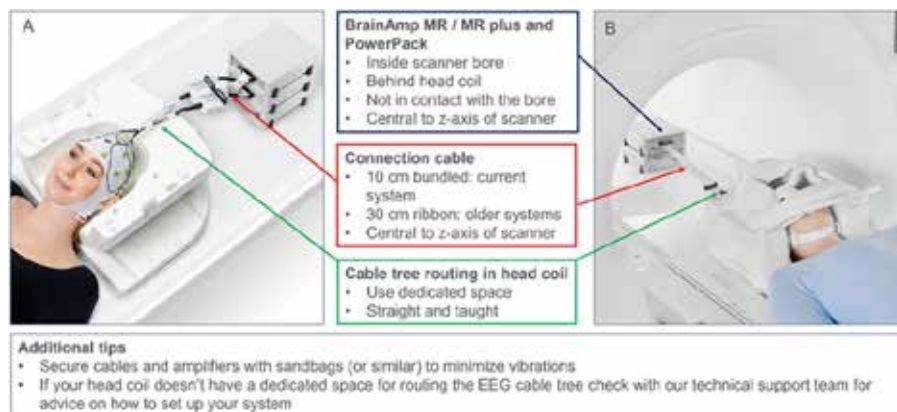
Figure 2. How to position the BrainAmp MR (plus) system inside the scanner bore. Part A shows a BrainCap MR with CWLs inside a head coil, the top part of the head coil is removed to show the dedicated space for the EEG cable tree. 10 cm bundled cables are used to connect the EEG cap and CWLs to the amplifiers. Part B shows the full head coil and the BrainAmp MR plus and PowerPack positioned behind the head coil on a platform inside the scanner bore. A 30 cm ribbon cable is used to connect the EEG cap to the amplifier.

BRAIN**VISION**
professional **BRAINAMP MR**

BRAIN**VISION**
professional **BRAINAMP MR PLUS**

BrainAmp MR and BrainAmp MR plus
Superior solutions for recording EEG in the MR

Our BrainAmp MR amplifiers are gold standard solutions for simultaneous EEG-fMRI co-registrations. They have been on the market since the early 2000s and their extremely high data quality (in the MR and the lab environment), their ease of use, as well as unparalleled scientific and technical support make them a first choice for researchers around the world. There are hundreds of scientific publications in the EEG-fMRI field citing our BrainAmp MR amplifiers and the number is still growing.

The BrainAmp MR amplifiers are technologically superior shielded amplifiers, which can be taken directly inside the MRI chamber and placed in the bore directly behind the participant's head. From the amplifier, the digitized signal is sent via fiber optic cable to the USB interface located in the control room. Therefore, no artifacts are accumulated along the way to the outside of the MRI chamber. The short length of the electrical cable used to connect the electrode cap with the amplifier fulfills all safety requirements for the participant and guarantees an outstanding data quality. The BrainAmp MR series are subject to our general EEG-fMRI safety guidelines.

The BrainAmp MR and MR plus features translate into a multi-functional, versatile, state of the art amplifier that can be combined with the BrainAmp ExG MR to add capability to record bipolar and peripheral signals such as EOG, ECG, EMG, GSR/EDA, respiration and acceleration in a compact setup. The BrainAmp system has successfully been used for simultaneous EEG-fMRI acquisitions, EEG-fMRI-PET acquisition, EEG/TMS co-registrations and for EEG/ERP studies, as well as for Brain Computer Interface (BCI) applications.

The BrainAmp MR plus includes all features of the BrainAmp MR with the addition of a DC recording mode and multiple hardware filtering options. The amplifier setup is fully controllable via the recording software.

BrainAmp MR and MR plus systems are powered by the rechargeable PowerPack battery. Multiple amplifiers can be combined to increase the maximum number of available channels to 128 for recordings in the MRI environment and up to 256 channels for laboratory applications. The BrainAmp amplifiers are compatible with passive gel-based electrodes (BrainCap MR) or passive sponge-based electrodes (R-Net-MR).

BrainAmp ExG MR
MR Compatible bipolar amplifier with unparalleled design

Measuring peripheral physiological signals during fMRI can add valuable insight into the physiological processes that occur in parallel to changes in the brain. For example, measures of arousal and muscle movements can provide complementary data. Respiration rate can be measured to control for vasomotion effects in both the EEG and fMRI data. Our BrainAmp ExG MR can be used to record bipolar signals such as surface EMG and ECG and signals from peripheral physiology sensors measuring GSR, respiration, or acceleration can be recorded using auxiliary channels. The BrainAmp ExG can also be used in combination with Carbon Wire Loops attached to EEG caps to measure potential artifacts in the EEG data such as movement and vibrations in the scanner bore. The peripheral signals measured by the BrainAmp ExG MR are directly integrated with the EEG signal in our recording software. Our EEG-fMRI setup ensures synchronous timing of the two modalities allowing easy and accurate comparison of the physiological data with the fMRI time series.

The BrainAmp ExG MR is a bipolar amplifier which means that the potential difference between a pair of electrodes is measured. The BrainAmp ExG MR can be used to record peripheral signals alongside EEG or as a standalone measurement. The 8-channel BrainAmp ExG MR has eight bipolar channels for signals such as surface EMG, ECG, EOG, and movement-related signals from Carbon Wire Loops. The 16-channel BrainAmp ExG MR has eight bipolar channels and eight auxiliary channels. The auxiliary channels allow input form peripheral physiology sensors measuring GSR, respiration, or acceleration.

The BrainAmp ExG MR is powered by the rechargeable PowerPack and is accompanied by the ExG AUX Box which allows for connecting MR compatible electrodes and sensors.

The state-of-the-art setup for combined EEG and fMRI recordings

Our optimized EEG-fMRI setup enables the integration of multiple physiological signals acquired in the scanner, while maintaining accurate timing and high data quality recordings. The EEG-fMRI setup includes the SyncBox, USB 2 Adapter, the PowerPack, and the optional TriggerBox. Safe recording with our MR-compatible setup, including BrainCap MR, R-Net MR, and BrainAmp MR amplifiers (MR, MR plus, ExG MR) requires close adherence to our safety instructions (see the support tip section), which can be found on our website.

SyncBox

An integral tool designed to boost data quality for concurrent EEG and fMRI recordings

The SyncBox is a unique tool which significantly reduces timing related errors and increases the quality of MRI artifact correction by synchronizing the clock of the recording system with the clock driving the MRI scanner's gradient switching system.

Phase synchronization between the EEG equipment and the MRI scanner results in temporal stability of the EEG acquisition in relation to the switching of the gradients during the MR acquisition. This leads to significant improvements in MRI artifact correction and, therefore, tremendously increases the quality of the recorded data.

The SyncBox's scanner interface and the appropriate clock output available in the scanner electronics cabinets are physically connected by using a galvanic coupling device to avoid any potential influence on the MR scanner system.

Hundreds of Brain Products users have already chosen this solution and are experiencing the added advantage in using it together with all major commercial MRI scanners available on the market. If you would like to optimize your data quality, join the crowd!

USB 2 Adapter

Adapter

The USB2 Adapter (also known as BUA) serves as a USB interface to connect any BrainAmp amplifier with the recording computer. It is part of the standard delivery for the BrainAmp DC, BrainAmp MR, BrainAmp MR plus and BrainAmp ExG MR (stand-alone version). The BUA allows for the integration of physiological signal from peripheral sensors, noise signal from carbon wire loops and EEG signal in the recording software.

PowerPack

MR usable rechargeable batteries

The PowerPack is an MR usable rechargeable battery designed for use with BrainAmp MR, BrainAmp MR plus, BrainAmp Standard, Brain Amp DC, BrainAmp ExG and BrainAmp ExG MR systems. The PowerPack is the perfect solution for safe EEG recordings in the MR. It is also a valid alternative to the mains power systems for standard EEG/ERP recordings as it fully eliminates problems with 50/60 Hz noise. The PowerPack can supply two amplifiers for up to 15 hours and has a deep discharge protection when in use. Assuming that the PowerPack is connected to a charging source when not in use, the PowerPack is an extremely economic and long-lasting purchase.

TriggerBox

An indispensable tool to easily handle and merge triggers from various sources.

The TriggerBox helps handle and merge triggers arriving from different sources, which is quite often a requirement in complex setups. For example, some markers might arrive from experimental control software via parallel -BD25 (LPT port) – input while other devices may communicate through BNC. If so, the amplifier should record all the triggers simultaneously. The TriggerBox also has one port that can stretch triggers, which may be necessary to receive volume triggers of an appropriate length from some MR interfaces. The TriggerBox Extension offers 8 additional BNC connectors which can be linked to the 8 upper bits (from line 8 and 15) of any BrainAmp amplifier. To use the TriggerBox as a virtual serial port, the installation of a small application, the TriggerBox IO, is required. The TriggerBox and TriggerBox Extension serve as a general adapter which replaces many small adapters, cables and boxes and thus are a useful addition to any lab.

Sensors for MR

Measuring peripheral physiological signals during fMRI can add valuable information about physiological processes to your studies. For example, measures of arousal or muscle movements could provide complementary data to the EEG and/or fMRI data. Our range of MR sensors allow you to easily add such measures to your research when used in combination with the BrainAmp ExG MR.

As one of the leading providers for solutions in EEG research, we have designed several types of MR compatible electrodes and sensors to measure acceleration, galvanic skin response, respiration, surface EMG and EOG, and non-physiological and physiological movement in the MR environment. In combination with the BrainAmp ExG MR, peripheral signals are incorporated with our MR standard setup to ensure high quality data and accurate scanner artifact removal. All MR-compatible sensors and equipment require close adherence to our safety instructions, which can be found on our website.

BRAINVISION
professional **GSR MR**

GSR (Galvanic Skin Response) module for fMRI

The GSR MR sensor measures skin conductance (SC), which is one of the most employed measures in psychophysiological research. As a sensitive parameter for emotional and cognitive states, stress and pain, SC has also been widely used in psychiatric research.

The GSR MR Sensor measures skin conductance using the exosomatic recording principle with direct current (DC) This means that a constant voltage of 0.5 V is applied in order to acquire the skin conductance. The sensors consist of 2 surface electrodes and a GSR module, that converts the electric SC to a voltage recorded by a bipolar amplifier input.

The sensor interfaces with the bipolar BrainAmp ExG MR via the ExG AUX box and the GSR is recorded synchronously with the EEG. Because of the high CMRR interface properties, the gradient artifact emerges remarkably suppressed, so that in many cases smoothing is sufficient to get a laboratory-like GSR signal.

3D Acceleration Sensor MR

The 3D Acceleration Sensor MR captures movements in three dimensions. The primary application of the Acceleration Sensor is to detect and record movement and acceleration of the extremities.

The module is made up of the sensor and a preamplifier. Two sensors with cables of different lengths are supplied as standard. This is intended to ensure that the cables are routed in the best possible fashion. The sensors are connected to the ExG AUX Box and BrainAmp ExG MR amplifier, allowing integration with other recording modules.

Multitrode MR electrodes for surface EMG

Measures of arousal or muscle movements through surface EMG electrodes can provide complementary data. For surface EMG measurements we offer bipolar multitrode MR electrodes. They have some special features that make them suitable for use in the MR environment: they have a current-limiting resistor, they are an incomplete ring to avoid induced eddy currents, and are bundled in a spiral tube so that the lead wire cannot come into direct contact with the participant.

Because surface EMG signals can be measured at a wide variety of sites on the body and in contrast to EEG measurements, where the electrode position and lead wire routing is determined by the electrode cap, the position and routing of surface EMG electrodes can result in a great deal of variability in possible configurations. We recommend that you consult our support tips on our website or to get in touch with the support team to ensure a safe EMG setup.

BRAIN VISION
professional **RESPIRATION BELT MR**

Respiration Belt MR

a device for parallel respiratory measurements

Respiration plays a critical role in the MR environment, as it may not only be a confounding factor, but also a source of related artifacts. It can be linked to movement artifacts, physiological alterations, induced field inhomogeneity, or interference with the experimental paradigm. Therefore, respiratory effects cannot be ignored [1].

The Respiration Belt MR consists of an elastic belt with a pouch, a pneumatic sensor, a transducer and a cable for the connection to the amplifiers' auxiliary ports. It measures the thoracic or abdominal respiratory movements and converts them into electrical voltages.

The compatibility and safety of the Respiration Belt MR result from its technical characteristics. Namely, it is based on a pneumatic technology, unlike most solutions on the market. This avoids safety issues related to the introduction of electrical devices in strong magnetic fields; therefore, it is not a source of artifacts for the MR imaging, thus preserving the highest data quality and ensuring that no noise is induced in the MR recorded signal.

References

[1] Thomason Moriah E., Burrows Brittany E., Gabrieli John D.E., Glover Gary H., Breath holding reveals differences in fMRI BOLD signal in children and adults, NeuroImage, Volume 25, Issue 3, 15 April 2005, Pages 824-837, ISSN 1053-8119, 10.1016/ j.neuroimage.2004.12.0

Carbon Wire Loops
State of the art MR artifact handling

Carbon Wire Loops (CWLs) are an innovative solution to remove noise induced by the MR environment from EEG signal. Predictable artifacts that repeat regularly, such as the gradient artifact, can be removed from EEG data acquired during fMRI scanning using an average template subtraction approach. On the other hand, motion-related artifacts, are non-cyclical and unpredictable, thus requiring a different approach for correction.

Movement-induced signals including movements from the subject, cardio ballistic artifact, and vibrations from the ventilation system and helium pump, can be measured by a loop moving inside a magnetic field. The CWLs can be attached to the BrainCap MR and R-Net MR to obtain reference signals inside the MR scanner. The small movements of these CWLs in the magnetic field generate signals that can then be used to estimate and remove motion artifacts from the EEG.

The CWL solution contains 4 loops situated at the frontal-left, frontal-right, parietal-left, and parietal-right locations and can be used in MRI scanners up to 3 T. Because the loops are bipolar, a BrainAmp ExG MR amplifier will be needed to record these signals. If you would also like to measure other bipolar or auxiliary peripheral signals at the same time, you will need a second BrainAmp ExG MR: one amplifier positioned at the head for the CWL measurements and one position at the foot end for the peripheral physiology measurements. The use of CWLs is subject to our general 3 T EEG-fMRI safety guidelines.

BrainCap MR
Superior electrode system for simultaneous EEG-fMRI

The simultaneous recording of EEG-fMRI is a well-established technique and our MRI product portfolio is the gold standard for this application. We strive to keep our products up to date to guarantee the highest safety and comfort for the participant as well as outstanding data quality. As such, our BrainCap MR Rev.3 (from April 2020) has evolved in recent years to keep up with the demands of this dynamic research area.

All the electrodes in the BrainCap MR are fitted with serial current-limiting resistors. The electrode cables are routed on the outside of the BrainCap MR and are secured to the cap so that loops are not formed and cable movement is avoided. The drop-down electrodes (e.g., ECG) are sheathed in plastic to avoid direct contact with the skin of the participant. Wire length from electrode to the amplifier is fixed to the minimal required length. Cable tree exit points are available to fit with different MRI head coils.

Flat electrode holders are used to guarantee the comfort of the cap, especially when the head of the test subject in supine position is resting on the electrodes. Caps with less than 64 channels contain spare electrode holders to compensate for gaps between the electrodes. This increases the number of contact points between the test subjects' head and the MRI scanner head-rest to further decrease discomfort.

Additionally, the BrainCap MR can be equipped with Carbon Wire Loops (CWL) for better correction of motion related artifacts. The CWLs are bipolar channels and the measurement requires a BrainAmp ExG.

BRAIN VISION
professional **R-NET MR**

R-Net MR

Sponge-based electrode system for simultaneous EEG-fMRI able batteries

The addition of the R-Net MR to our MRI product portfolio provides flexibility to choose the right electrode system for your research needs. The R-Net MR consists of saltwater sponges and passive Ag/AgCl electrodes housed in durable and flexible silicone structure. The MR version of the R-Net also has current-limiting resistors for safe recordings in the MRI environment and a gel-based ECG electrode. The R-Net MR is available for BrainAmp MR amplifiers and can be used in scanners up to 3T. Its use is subject to our general 3 T EEG-fMRI safety guidelines.

All the electrodes in the R-Net MR are fitted with serial current-limiting resistors. The electrode cables are routed on the outside of the R-Net MR and are secured to the cap so that loops are not formed and cable movement is avoided. The ECG electrodes contain higher resistors than EEG electrodes and the lead wire is made of carbon to compensate for the technical characteristics of longer wires. The ECG drop-down electrode is sheathed in plastic to avoid direct contact with the skin of the participant. Wire length from electrode to the amplifier is fixed to the minimal required length. Cable tree exit points are available to fit with different MRI head coils.

The R-Net MR offers a quick EEG setup with no skin preparation and gel residues. The R-Net is a good choice for applications in which fast preparation is essential. Whereas the gel in gel-based electrode systems reduces impedance between the skin and electrode, allowing for a higher quality signal to be recorded.

The R-Net MR is available in configurations of 32, 64, 96, and 128 channels. In addition, the R-Net MR can be equipped with Carbon Wire Loops (CWL) for better correction of motion related artifacts. The CWLs are bipolar channels and the measurement requires a BrainAmp ExG MR.

BrainVision Analyzer 2

Our answer for today and tomorrow

Our market leading complete EEG & ERP processing software with more than 20 years on the market and in use by labs worldwide. It is self-documenting, easy to use, and comes with a variety useful tools. Its unique History Tree® structure for analysis and powerful features with MATLAB® integration, Wavelet analysis, ICA and many more make it the perfect tool for analyzing data from nearly any EEG amplifier available on the market. The analysis software comes with specific transformations for handling MR-acquired EEG and peripheral physiological data. Gradient artifacts and cardioballistic artifacts can accurately be removed with the moving average template subtraction algorithm implemented in BrainVision Analyzer. Furthermore, movement-related signals and cardioballistic artifacts acquired with Carbon Wire Loops can easily be removed from the EEG with our CWL multivariate regression ensuring the highest data quality.

BrainVision Recorder

Easy to use multifunctional recording software

The BrainVision Recorder controls all our amplifiers, displays and saves the incoming data and trigger information, including MR volume, synchronization and paradigm triggers. A very convenient wizard menu structure guides you through the entire hardware setup and hardware/software filter configuration.

Channel impedances can easily be checked and are automatically stored along with all acquisition parameters. Various options such as online averaging or video integration are available. BrainVision Recorder software can be easily interfaced with other software solutions like Presentation® and E-Prime.

BrainVision RecView

Software for real-time data analyses

BrainVision RecView is an advanced solution designed for real-time analysis of data received over the Ethernet network via TCP/IP directly from the Recorder software. BrainVision RecView is widely used for EEG-fMRI co-registration to remove both the gradient and the ballistocardiogram artifact giving insight into data quality in real time and permitting experimental control during the scan.

By using the same History Tree® concept already implemented in BrainVision Analyzer 2, RecView can also be used for FFT analysis, data filtering, mapping of the surface potentials as well as BCI and bio-/neurofeedback of the incoming data.